7. Formulation Development of Microneedle Patches

7.1. Introduction

As it is known that stratum corneum proves to be barrier for the permeation of drugs through the skin. So, to overcome this barrier and achieve permeation of drugs in deeper layers of skin, optimized nanocarriers were loaded into fast dissolving microneedles. Additionally, they also can deliver potent drug molecules through the skin in the most precise manner. A major advantage of fast dissolving microneedles is the negligible risk of damage or cross-contamination. This damage or cross-contamination has been observed in other metal or non-biodegradable microneedles.(1-3) A simplified micromold casting method was used for fabrication of fast dissolving microneedle patches that requires less production time and cost and holds promise for large scale production.(1) A systematic Quality-by-design (QbD) approach employing statistical design of experiments was utilized to exhaustively evaluate the impact of material attributes and process parameters on the vital formulation parameters.(4)

7.2. Materials and Methods

7.2.1. Materials

Ami drugs and specialty chemicals Pvt. Ltd., India and Concord Biotech Ltd., India gifted samples of FBX and TAC respectively. DermaStamp DTR-150 and YYR-150 (35 and 80 titanium microneedles respectively) were procured from Guangzhou Junguan Beauty Co. Ltd., China. Poly-dimethylsiloxane (Sylgard® 184) was procured from Dow corning, USA. Poly vinyl alcohol (MW, 6 kD) and Lactose (MW, 3.5 kD) were procured from Acros organics, Mumbai, India and Hi-Media respectively. The components required for the transdermal patch such as backing film, high adhesion double coated medical tape and release liner were gifted by Mill Laboratories Pvt. Ltd., Vadodara, India. Double distilled water was prepared in lab, which was filtered with the help of 0.2µ membrane filter in glass bottle and consumed within a maximum of 7 days.

7.2.2. Preparation of poly-dimethylsiloxane (PDMS), a secondary micromoulds

Micromoulds of poly-dimethylsiloxane (PDMS) were prepared using 35 and 80 titanium microneedles dermastamp (DTR-150 and YYR-150) as master templates. Briefly, silicone elastomer and curing agent were taken in a weight ratio of 10:1 and was then mixed. Further this mixture was transferred in a suitable molding containers made of high density plastic. The master templates were carefully inserted into the containers avoiding any air bubble and kept overnight at room temperature for partial curing. After 12 hours, master templates were removed and micromoulds were completely cured at 90°C for 8 hours in a water-bath. The micromoulds were separated from containers and used for fabrication of fast dissolving microneedle patch.(5)

7.2.3. Preparation and optimization of cubosomes loaded fast dissolving microneedle patch

Preparation MN patch containing cubosomes of TAC

For the preparation of microneedle matrix, polyvinyl alcohol (PVA) was used as a binder in the concentration of 35% w/v and Lactose was used as a filler at the concentration of 5% w/v. Hot plate magnetic stirrer was employed for solubilizing optimum amounts of PVA and lactose in 10 ml of TAC cubosomal dispersion (3.3 mg/ml TAC). This mixture was gently stirred at a temperature of 50 °C on the hot plate magnetic stirrer. Further this mixture was cooled and was brought back to ambient room temperature. The resulting 0.6 mL of PVA/Lactose blend solutions which contain approximately 2 mg of drug were shifted into PDMS micromolds which have capacity of around 0.6 mL (dimension of mold is 1.5 X 1.5 cm). In order to fill the cavities of microneedles of the micromolds, it was centrifuged set at an rpm of 3000 at 25 °C for 10 minutes using Remi Centrifuge (model-CPR 30). Further, to ensure that the microneedle structure was properly hardened, micromolds were placed in vacuum desiccators for a period of 24 hours to evaporate the water. 1567 high adhesion double sided medical tape (3M™, USA) which had backing film on the opposite adhesive side was employed to extract the microneedle arrays from micromolds. MN Patches

prepared from the aforesaid procedure were kept in airtight containers and calcium oxide along silica gel was employed as desiccants.(5, 6)

Preparation MN patch containing cubosomes of FBX

For FBX 10% w/v lactose was used in place of 5% w/v because more amount of cubosomal dispersion was needed due to the high dose of FBX. The cubosomes are vesicular systems due to which MN became elastic in nature, so to provide enough strength more lactose was needed. For the preparation of microneedle matrix, polyvinyl alcohol (PVA) was used as a binder in the concentration of 35% w/v and Lactose was used as a filler in the concentration of 10% w/v. Hot plate magnetic stirrer was employed for solubilizing optimum amounts of PVA and lactose in 10 ml of FBX cubosomal dispersion (3.4 mg/ml FBX). This mixture was gently stirred at a temperature of 50 °C on the hot plate magnetic stirrer. Further this mixture was cooled and was brought back to ambient room temperature. The resulting 1 mL of PVA/Lactose blend solutions which contain approximately 3.4 mg of drug were shifted into PDMS micromolds which have capacity of 2 mL (dimension of mold: 1.5 X 3.0 cm). In order to fill the cavities of microneedles of the micromolds, it was centrifuged at rpm of 3000 at 25 °C for 10 minutes using Remi centrifuge (model-CPR 30). Further, to ensure that the microneedle structure was properly hardened, micromolds were placed in vacuum desiccators for a period of 24 hours to evaporate the water. 1567 high adhesion double sided medical tape (3M™, USA) which had backing film on the opposite adhesive side was employed to extract the microneedle arrays from micromolds. MN Patches prepared from the aforesaid procedure were kept in airtight containers and calcium oxide along silica gel was employed as desiccants.(5, 6)

7.2.4. Quality target product profile and critical quality attributes of formulation

Firstly, QTPP for cubosomes loaded MN patch of TAC/FBX was established on the basis of scientific, therapeutic, industrial and regulatory factors. Then, two response variables, axial fracture force (AFF) and dissolution time

were selected as CQA and this selection was done dependent on experimental trials, prior knowledge and literature review.

7.2.4.1.Axial Fracture Force (AFF)

Brookfield CT3 texture analyzer was employed for the measurement of axial needle fracture force. For performing this, double sided adhesive tape was used for placing microneedle arrays on the texture analyzer's mobile probe. This step was performed carefully in a manner that axis of microneedles aligns parallel with axis of mobile probe. After this, probe was automated for pressing the microneedles on a rigid, flat steel.(7) For testing the needle strength, graph made with the help of Texture Pro CT data acquisition software were employed.

7.2.4.2.*In-vitro* dissolution time

Preparation of gelatin slab

Stratum corneum exhibits a water content of approx. 30 ± 5 %. To simulate the conditions of stratum corneum, artificial gelatin skin was designed having a similar hydration level. This was achieved by adding 35% water and 65% gelatin.(5) For preparing the artificial gelatin skin, 6.5 g of gelatin was taken and was transferred in 10 ml water and this solution was kept for hydration for a period of 30 minutes. Further, gelatin was solubilized with the help of water bath at a temperature at 60 ˚C with continuous stirring. The resulting solution was transferred into a glass petridish and the water was permitted to vaporize till a weight of 10 g was attained. The resulting film obtained after evaporation was cut out to obtain small pieces having square shape.(5, 8)

In-vitro dissolution time

Optimized batch of MN patch was implanted in the gelatin film and re moved at various time intervals (15 & 30 second, 1, 1.5, 2, 2.5, 3, 3.5, 4, 4.5, & 5 min) and viewed under microscope.

7.2.5. Identification of independent variables and qualitative risk assessment using Ishikawa diagram

All possible variables which were linked with the development of fast dissolving MN patch were demonstrated with the help of Ishikawa diagram.

These factors were classified into three classes i.e. 'low, intermediate and high risk' depending on their predicted effect over CQA as described in Table 7.1.

Table 7.1: Quality risk assessment criteria for various attributes

Low Risk	Factors with wide range of acceptability. No investigation required.
Moderate Risk	Acceptable risk. Small change does not significantly affect the quality of product
High Risk	Unacceptable risk. Acceptable range of attributes needed to be studied.

7.2.6. Formulation optimization of fast dissolving microneedle patch using 3^2 Factorial Design

For explicitly studying the relation between the vital factors and CQA of fast dissolving MN patch, 3^2 Factorial Design was employed. This facilitated the use of reduced no. of experimental batches even though mixture components & other numeric factors could be handled concurrently.(9) A randomized design matrix was generated, experimental data was statistically evaluated for achieving an optimized solution and the design space was created by using Design Expert® 7.0.0. Software was employed for selecting a suitable model for the study. Analysis of variance was performed which was followed by F-test for the identification of significant model terms. CQA was calculated with the help of mathematical equations wherein, the equation was simplified by the removal of insignificant terms. The correlation among critical factors & CQA was studied with the help of contour & 3-D response surface plots. For the verification of the model, 3 batches of the optimized composition were formulated.(9)

7.2.7. Preparation of checkpoint batches as per the overly plot

After adding the data of the prepared batches advised by the 3^2 factorial Design, this data was analyzed at 95 % confidence and prediction level using Design Expert 7.0 for the optimized area.(9) Three randomized point were selected from this optimized area and checkpoint batches were prepared according

to it. The composition of this checkpoint batches for cubosomes loaded MN patches of TAC/FBX are given in table 7.2 & 7.3.

Table 7.2: Composition of checkpoint batches for cubosomes of TAC loaded MN Patch

Sr. No.	Concentration PVA (% w/v)	Concentration of lactose (%w/v)	AFF (N)	Dissolution time (s)
1	32.36	4.35	0.83	1.13
2	35.79	4.52	1.18	1.43
3	30.99	1.60	0.81	1.66

Table 7.3: Composition of checkpoint batches for cubosomes of FBX loaded MN Patch

Sr. No.	Concentration PVA (% w/v)	Concentration of lactose (%w/v)	AFF (N)	Dissolution time (min)
1	31.28	9.56	0.73	0.92
2	34.80	9.34	1.23	1.22
3	34.31	7.19	0.60	1.68

7.2.8. In vitro characterization of optimized cubosomes loaded fast dissolving Microneedle patch

7.2.8.1.Axial Fracture Force

Axial fracture force was measured as described in section 7.2.4.1.

7.2.8.2.In-vitro dissolution time

In-vitro dissolution study of prepared MN Patch was performed as described in section 7.2.4.2.

7.2.8.3.Shape and surface morphology

For characterization of microneedles shape and their surface morphology, fast dissolving MN Patch were affixed on sample stub and observed under JSM-5610LV scanning electron microscope (JEOL, Japan) wherein the accelerating voltage is set at 20 kV.(5)

7.2.8.4.Skin penetrability

For checking the skin penetrability, double sided adhesive tapes were employed for mounting the microneedles on mobile probe of Brookfield CT3 texture analyzer. Care was taken that the axis of microneedle is aligned parallel with the axis of the mobile probe. Probe was automated for pressing the microneedles on the full thickness of pinned pig ear skin on a soft sponge pad under slight tension for simulating in-situ mechanical support. The insertion speed of the moving probe was set at a speed of 20 mm/s. Skin area which was treated with microneedle was treated with trypan blue dye for a period of 5 minutes. A tissue paper was used for wiping off the excess dye from the skin. Further, digital camera was employed for taking the pictures of stained pores.(8)

7.2.8.5.Pore closure kinetic

For performing this study, rat skin was pinned with slight tension onto the soft board, for simulating in-situ mechanical support. Then, Fast dissolving MN Patch was applied on the skin for 0, 3, 6, 12 and 24 hours. At each time point, MN Patch was detached and sections of epidermis were taken using cryo-microtome to observe for pore closure with the help of Eclipse H600L inverted microscope (Nikon, Japan).(8)

7.2.8.6.Physical stability of cubosomes in fast dissolving microneedle patch

After preparing the fast dissolving MN Patch, instantly the physical stability of the cubosomes in MN Patch was examined. The size and entrapment efficiency of dispersion of cubosomes was evaluated with the help of methods mentioned in earlier chapters 5.2.9.3, 5.2.9.4, 6.2.9.3, and 6.2.9.4. For this, the MN Patch was solubilized in pre-filtered distilled water for obtaining the dispersion of cubosomes.(8)

7.2.8.7.Total drug content

Double distilled water was taken in a volume of 10 ml and used for solubilizing prepared MN Patches of TAC and FBX. Then, 1 ml of prepared samples were diluted with acetonitrile and acetonitrile: Methanol (9:1) respectively and quantitatively analyzed using the analytical method described in chapter 3.(8)

7.2.8.8.*In vitro drug release*

Franz-type diffusion cells of 2 different capacities, i.e. 20 ml (for FBX) and 7 ml (for TAC) of the receptor chamber was employed for studying the in-vitro release from fast dissolving MN Patch loaded with nanocarriers. For designing the experiment, pre-activated dialysis membrane (MWCO, 12 kD) which is to act like a permeation barrier is affixed amid the donor & receptor compartments. Further, a diffusion medium i.e. 1 % ethanolic phosphate buffer pH 7.4 was transferred into the receptor compartment. The diffusion cell was left undisturbed for half an hour to facilitate equilibration between receptor and donor compartments. In-vitro drug release study of plain drug suspension in water (2 mg/ml), plain drug containing microneedle patch (2 mg), and microneedles patch containing cubosomes of TAC (2 mg) was performed by placing these in the donor compartment. Samples were taken from the receptor compartment in a volume of 0.5 mL at regular intervals (0.5, 1, 2, 3, 4, 5, 6, 12 and 24 hour). Additionally, the same volume i.e. 0.5 ml of fresh diffusion medium was added in the receptor compartment. Samples were evaluated using developed HPLC method as described chapter 3. Triplicate readings of all experiments were recorded and further average of these readings was considered.(3, 8, 10)

Same procedure was followed 1 % ethanolic phosphate buffer as a diffusion medium for the in-vitro release study of FBX using 20 ml of Franz diffusion cell. For this study, plain drug suspension in water (3.4 mg/ml), plain drug containing microneedle patch (3.4 mg), and microneedles patch containing cubosomes of FBX (3.4 mg) were placed in donor compartment of Franz diffusion cells. Triplicate readings of all experiments were recorded and further average of these readings was considered.

7.3. Results and Discussion

7.3.1. Micromoulds Preparation

Process used for micromould formation and characterization is illustrated in Fig. 7.1. PDMS micromoulds were prepared exactly complimentary to the

master structure. Microscopic evaluation of micromoulds showed smooth and conical microneedle cavities.

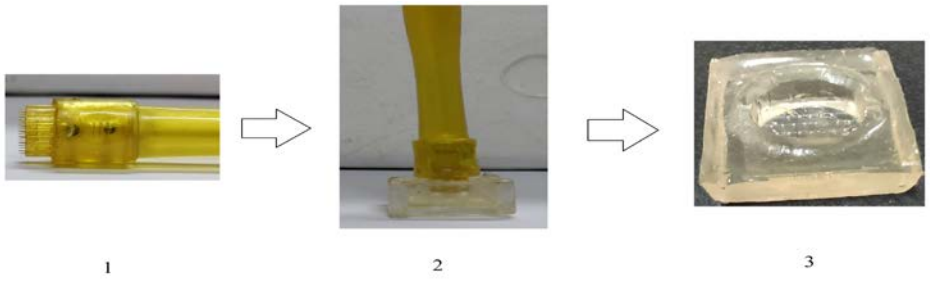

A

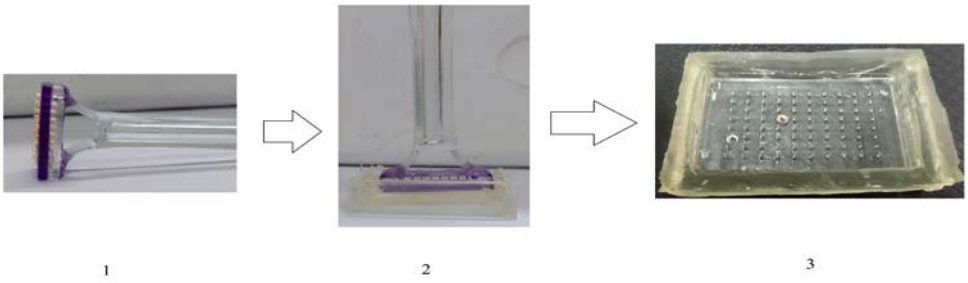

B

Figure 7.1: Process for preparing micromould to prepare (A) TAC MN patch (B) FBX MN patch. In figure, 1 indicate dermastamp, 2 indicate dermastamp hold in primary (casting) mould and 3 indicate secondary micromould.

7.3.2. Quality target product profile and critical quality attributes of formulation

Various Quality target product profiles and their targets were identified and listed in table 7.4 with proper justification.

Table 7.4: QTPP elements of fast dissolving MN Patch with their justification

QTPP parameter	Target	Justification
Route of administration	Transdermal	To avoid first pass metabolism and gastro-intestinal related side effect associated with drug

Dosage form		Microneedle patch	Capable of permeating stratum corneum and enhance the drug permeation across the skin
Formulation quality target	Needle length	≤ 1.5 mm	To ensure breaching the stratum corneum with absence of pain
	Axial fracture force (AFF) of needle*	> 0.6 N	To ensure skin penetration of microneedle without breaking of needle
	Skin penetrability	Yes	To ensure penetration of skin to enhance drug permeation
	Surface characteristics	Smooth	For ease penetration
	In vitro dissolution*	Within 5 min	To ensure fast release of drug loaded cubosomes
Safety		Non-toxic and non-irritant to skin	To ensure complete safety of final prepared formulation

* Critical quality attribute

AFF of microneedle and in-vitro dissolution time were identified as critical quality attributes for the preparation of MN Patch. Thus, these attributes need to be controlled in order to obtain pre-defined Quality Target Product Profile.

7.3.3. Identification and qualitative assessment of independent variables

During the various brainstorming sessions, all likely variables related with development of fast dissolving MN Patches by micromold casting were

recognized and were categorized into these categories i.e. Personnel, Material, Environment, Process and Equipment.(11) Ishikawa diagram was constructed for illustrating the cause and effect relation between recognized variables and CQA (Fig. 7.2).

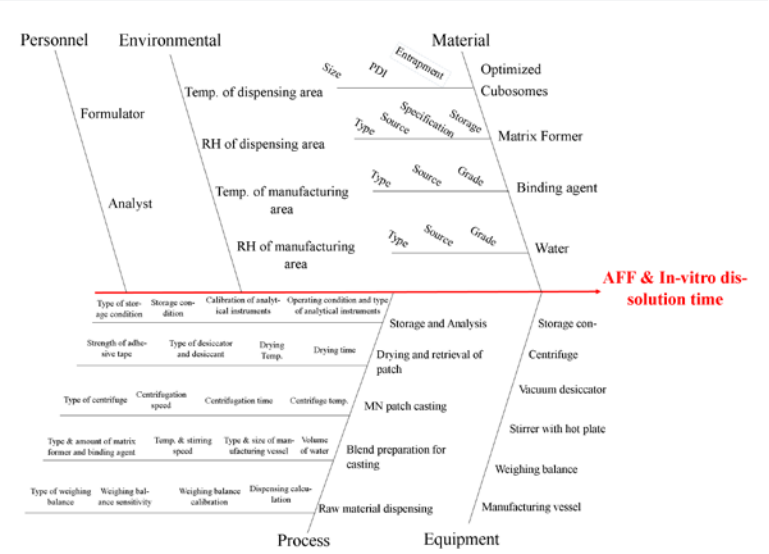

Figure 7.2: Ishikawa diagram showing probable variables that may influence the CQA

7.3.4. Qualitative risk assessment

The risk associated with all identified factors were evaluated based on predefined criteria (Table 7.1) and the result is presented in Table 7.4. Factors which are associated with low and intermediate risk were allocated with best possible constant levels. This allocation of constant levels was dependent on preliminary trials and literature. This was done to ensure no or minimal effect of these factors on CQA. These constant levels are also mentioned in Table 7.4.

Table 7.4: Qualitative risk assessment of independent variables

Factors	Process step	Impact on CQA	Constant level
Grade of water		Low risk	Double distilled filtered (0.2 µm) water
Weighing balance	Dispensing	Low risk	1 mg

sensitivity	area		
Weighing balance calibration		Low risk	Calibrated
Temperature and Relative humidity (RH) of dispensing area		Low risk	25 ± 3 °C, Ambient RH
Type, size and material of construction	Manufacturing vessel	low risk	20 mL class A borosilicate glass bottle
Temperature and RH	Manufacturing area	Low risk	25 ± 3 °C, Ambient RH
Volume of water	Preparation of casting solution	Low risk	10 mL
Amount of PVA		**High risk**	**Need to be optimized**
Amount of Lactose		**High risk**	**Need to be optimized**
Stirring speed and time of aqueous phase		Low risk	500 rpm, 20 min
Temperature of aqueous phase		Low risk	50 °C
Removal of air bubble from casting solution		Low risk	Removed by putting casting solution in vacuum desiccator for 30 min
Filling of microneedle molds	Microneedle fabrication	Low risk	Filled using calibrated microneedle pipette
Type of centrifuge		Low risk	Centrifuge with swing bucket rotor head
Centrifuge speed		Moderate risk	3100 rpm

Centrifuge time		Moderate risk	15 min, 3 cycle
Drying time	Drying of microneedle patch	Moderate risk	48 hours
Drying temperature		Low risk	Room temperature
Type of dryer		Low risk	Vacuum Desiccator with silica bag and calcium oxidase as desiccants
Adhesive tape	Microneedle removal from mold and patch formation	Low risk	High adhesive PU (polyurethane) double sided medical tape 3M
Release liner		Low risk	Scothchpak™ 9741 release liner, 3M
Backing membrane		Low risk	Scothchpak™ 9735 backing membrane, 3M
Storage condition	Storage and analysis	Low risk	At room temperature in Desiccator with silica bag and calcium oxide as desiccants
Calibration of analytical instruments		Low risk	Calibrated
Formulator	Personnel	Low risk	Common for all formulation steps
Analyst		Low risk	Common for all analytical procedure

Two factors were identified as high risk factors and were taken forward for formulation optimization.

7.3.5. Formulation optimization of cubosomes of Tacrolimus loaded Microneedle Patch by 3^2 Factorial Design

Based on qualitative risk assessment, two CMAs were identified and their relationship with CQAs were exhaustively investigated using 3^2 Factorial Design. 3^2 Factorial Design was found to be suitable as it facilitated the study of PVA and lactose along with numerous numerical number. The low (-1), medium (0) & high (+1) levels of all three CMA are listed in Table 7.5.

Table 7.5: Various critical material attributes along with their levels for optimization of cubosomes of TAC loaded MN Patch by 3^2 Factorial Design

Independent variables (CMA)		Unit	Levels		
			-1	0	+1
A	Concentration of PVA	% w/v	30	35	40
B	Concentration of Lactose	% w/v	1	2.5	5

A randomized matrix of thirteen batches was generated by Design-Expert 7.0 and presented in Table 7.6. These batches were formulated according to the respective run order and were studied for CQA using the methods described earlier. Table 7.5 also represents the resulting CQA of these batches.

Table 7.6: Randomized design matrix for cubosomes of TAC loaded MN Patch using 3^2 factorial design with its CQA

Batch no.	Run order	Independent variables		AFF (N)	In-vitro dissolution time (min)
		A: Conc. of PVA % W/V	B: Conc. of Lactose %W/V		
M1	7	35	3	0.94	1.75
M2	13	30	5	0.7	1.25
M3	4	40	3	2.65	3.50

M4	6	35	5	1.11	1.5
M5	9	40	5	3.49	2.25
M6	2	30	1	0.4	2.0
M7	1	40	1	2.94	4.25
M8	10	35	3	1.04	1.75
M9	11	30	3	0.53	1.25
M10	8	35	3	0.81	1.75
M11	5	35	1	0.86	2.75
M12	12	35	3	1.68	1.75
M13	3	35	3	0.66	1.5

` The experimental data of axial fracture force (AFF) and in-vitro dissolution time software suggests quadratic model for process order. Analysis of variance (ANOVA) was performed by the same software. The categorization of terms as significant or insignificant was done on the basis of the p-value i.e. model term having p-value less than 0.05 (α-level) is significant while others are insignificant.(11) Hierarchy based deletion of insignificant model terms was done to streamline the model and obtain reduced equation. ANOVA and coded coefficients of Full model for AFF are mentioned in Table 7.7 and Table 7.8, respectively.

Table 7.7: ANOVA of full quadratic model for AFF

Source	Sum of Square	Degree of freedom	Mean square	F Value	p-Value > F	
Model	9.48	5	1.90	39.08	< 0.0001	Significant
Conc. of PVA	6.39	1	6.39	131.66	< 0.0001	Significant
Conc. of Lactose	0.93	1	0.93	19.14	0.0033	Significant
AB	0.57	1	0.57	11.75	0.0110	Significant
A^2	1.25	1	1.25	25.81	0.0014	Significant

B^2	0.013	1	0.013	0.27	0.6223	Not Significant
Residual	0.34	7	0.049			
Lack of fit	0.024	3	0.080	3.20	0.1453	Not significant
Pure error	0.100	4	0.025			
Cor total	9.82	12				

As showed in ANOVA table, concentration of PVA, Lactose and interaction between them were found to affect AFF significantly. An insignificant lack-of fit showed the competence of the model in justifying the difference in the observations.

Table 7.8: Coded coefficients of full quadratic model for axial fracture force

Term	Full model		
	Coefficient	SE Coefficient	VIF
Intercept	0.86	0.091	-
A: Conc. of PVA	1.03	0.090	1.0
B: Conc. of Lactose	0.39	0.090	1.0
AB	0.38	0.11	1.0
A^2	0.67	0.13	1.17
B^2	0.068	0.13	1.17

Coefficients table for AFF showed VIF values near to 1 indicating that the predictors are not correlated and regression coefficients are well estimated.(12) Regression equation for full model in coded and uncoded units is presented as Eq. 7.1 & 7.2. The (+) and (-) symbol preceding every coefficient indicates direct/ inverse connection of the respective model term with AFF.

$$AFF = +0.86 + 1.03\ A + 0.39\ B + 0.38\ AB + 0.67\ A^2 + 0.068\ B^2$$

Equation- 7.1

Reduced model equation:

$$AFF = +0.86 + 1.03\ A + 0.39\ B + 0.38\ AB + 0.67\ A^2$$

Equation- 7.2

Regression equation for reduced model is presented in equation 7.3.

$$AFF = +0.86 + 1.03\ (\text{Conc. of PVA}) + 0.39\ (\text{Conc. of Lactose}) + 0.38\ (\text{Conc. of PVA})(\text{Conc. of Lactose}) + 0.67\ (\text{Conc. of PVA})^2$$

Equation- 7.3

Here, we observed that concentration of PVA and lactose have a positive effect on the AFF of MN patch loaded with cubosomes of TAC which means that as the concentration of PVA and lactose increases it also increases the AFF of MN patch loaded with cubosomes of TAC. Moreover, from reduced model 7.2 an interaction term B^2 was removed as its p value is greater than 0.05 as showed in table 7.7.

Model summary of AFF is mentioned in Table 7.9. A low SD value and high R^2 value symbolized an improved prediction of observations by the model. Predicted R^2 value was reported to be in close proximity with adjusted R^2 value for further supporting the prediction potential of the model.

Table 7.9: Summary of full quadratic model for AFF

Response	Full model			
	SD	R-sq	R-sq (adj)	R-sq (pred)
AFF (N)	0.22	0.9654	0.9407	0.7439

Four different residual plots viz., normal plot of residual, residual versus ascending predicted response values, residual versus experimental run order and predicted versus actual were generated for the AFF and presented in Fig. 7.3. It was observed that the data was normally distributed in normal plot as it could be seen that the residuals followed a straight line. Further, the prediction of constant variance was validated as random scattering with the absence of any megaphone pattern in residual versus predicted plot was seen. Likewise, absence of lurking variables was validation by the random scattering lacking any pattern in residual versus run plot. The selected model gave convenient assumption of the values given that the data points were consistently split by 45-degree line.(13)

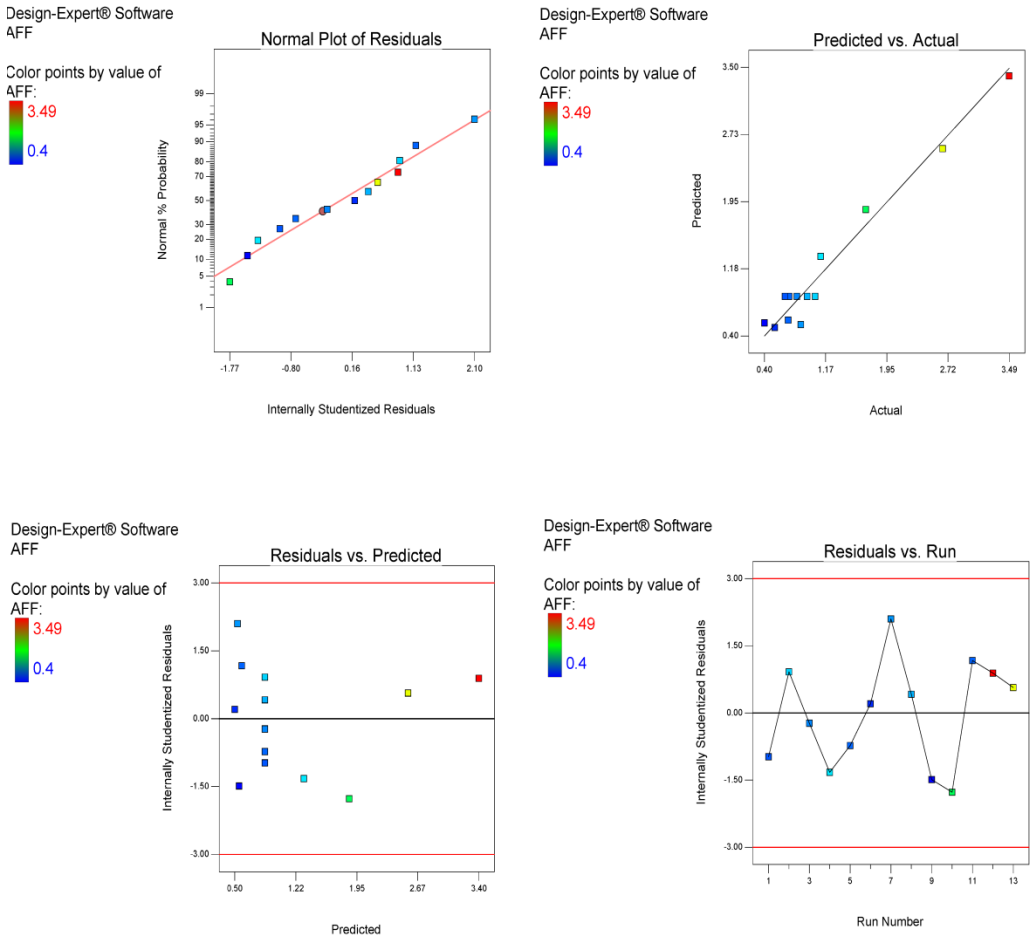

Figure 7.3: Residual plots for AFF of cubosomes of TAC loaded MN Patch

Contour and response surface plots are presented in Fig. 7.4. This graph was used to depict how AFF is related to respective CMA.

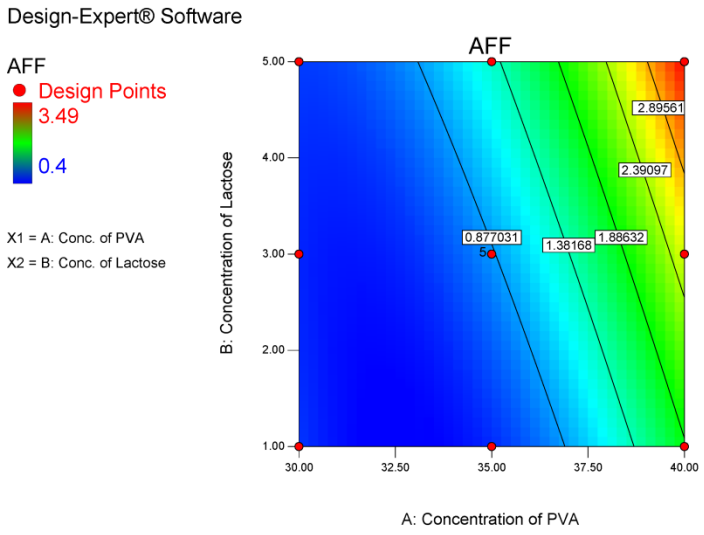

(A)

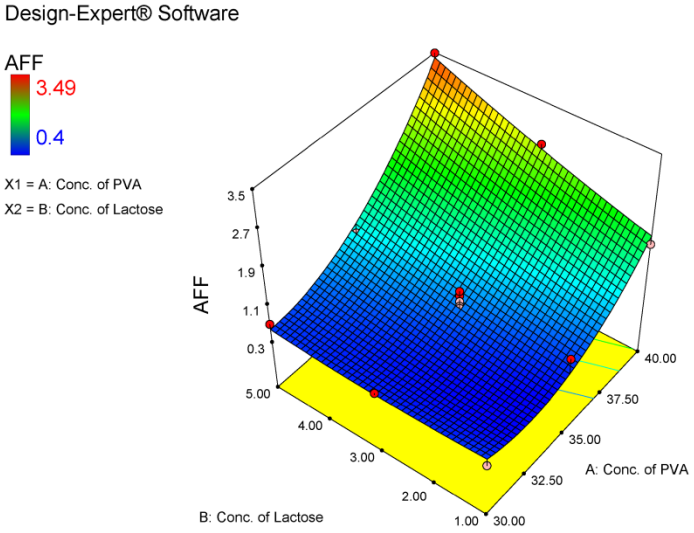

(B)

Figure 7.4: (A) Contour and (B) response surface plots for AFF of cubosomes of TAC loaded MN Patch

ANOVA and coded coefficients of Full model for in-vitro dissolution time are mentioned in Table 7.10 and Table 7.11, respectively.

Table 7.10: ANOVA of full quadratic model for in-vitro dissolution time

Source	Sum of Square	Degree of freedom	Mean square	F Value	p-Value > F	
Model	9.14	5	1.83	43.04	< 0.0001	Significant
Conc. of PVA	4.95	1	4.95	116.51	< 0.0001	Significant
Conc. of Lactose	2.67	1	2.67	62.76	< 0.0001	Significant
AB	0.39	1	0.39	9.19	0.0191	Significant
A^2	0.59	1	0.59	13.83	0.0075	Significant
B^2	0.15	1	0.15	3.63	0.0986	Not-Significant
Residual	0.30	7	0.042			
Lack of fit	0.17	3	0.057	1.84	0.2803	Not significant
Pure error	0.13	4	0.031			
Cor total	9.44	12				

As showed in ANOVA table, concentration of PVA, Lactose and interaction between them were found to affect in-vitro dissolution time significantly. An insignificant lack-of fit showed the competence of the model in justifying the difference in the observations.

Table 7.11: Coded coefficients of full quadratic model for in-vitro dissolution time

Term	Full model		
	Coefficient	SE Coefficient	VIF
Intercept	1.79	0.086	-

A: Conc. of PVA	0.91	0.084	1.0
B: Conc. of Lactose	-0.67	0.084	1.0
AB	-0.31	0.10	1.0
A^2	0.46	0.12	1.17
B^2	0.24	0.12	1.17

Coefficients table for in-vitro dissolution time showed VIF values near to 1 indicating that the predictors are not correlated and regression coefficients are well estimated.(12) Regression equation for full model in coded and uncoded units is presented as Eq. 7.4 & 7.5. The (+) and (-) symbol preceding every coefficient indicates direct/ inverse relationship of the respective model term with in-vitro dissolution time.

$$\text{In-vitro dissolution time} = +1.79 + 0.91\,A - 0.67\,B - 0.31\,AB + 0.46\,A^2 + 0.24\,B^2$$

Equation- 7.4

Reduced model equation:

$$\text{In-vitro dissolution Time} = +1.79 + 0.91A - 0.67B - 0.31\,AB + 0.46\,A^2$$

Equation- 7.5

Regression equation for reduced model is presented in equation 7.6.

$$\text{In-vitro dissolution time} = +1.79 + 0.91\,(\text{Conc. of PVA}) - 0.67\,(\text{Conc. of Lactose}) - 0.31\,(\text{Conc. of PVA})(\text{Conc. of Lactose}) + 0.46\,(\text{Conc. of PVA})^2$$

Equation- 7.6

From the equation 7.5, it can be concluded that concentration of PVA has a positive effect on the in-vitro dissolution time of MN patch means as the concentration of PVA increases in-vitro dissolution time of a MN patch also

increases. Opposite phenomena was observed with the concentration of lactose. Moreover interaction effect of concentration of lactose was not observed on in-vitro dissolution time of MN patch. Thus, in reduced model equation 7.6, interaction AB was removed because it has a p value greater than 0.05 as shown in table 7.10.

Model summary for in-vitro dissolution time is presented in Table 7.12. A low SD value and high R^2 value symbolized an improved prediction of observations by the model. Predicted R^2 value was reported to be in close proximity with adjusted R^2 value for further supporting the prediction potential of the model.

Table 7.12: Summary of full quadratic model for in-vitro dissolution time

Response	Full model			
	SD	R-sq	R-sq (adj)	R-sq (pred)
In-vitro dissolution time (min)	0.21	0.9685	0.9460	0.8150

Four different residual plots viz., normal plot of residual, residual versus ascending predicted response values, residual versus experimental run order and predicted versus actual were generated for in-vitro dissolution time and presented in Fig. 7.5. It was observed that the data was normally distributed in normal plot as it could be seen that the residuals followed a straight line. Further, the prediction of constant variance was validated as random scattering with the absence of any megaphone pattern in residual versus predicted plot was seen. Likewise, absence of lurking variables was validation by the random scattering lacking any pattern in residual versus run plot. The selected model gave convenient assumption of the values given that the data points were consistently split by 45-degree line.(13)

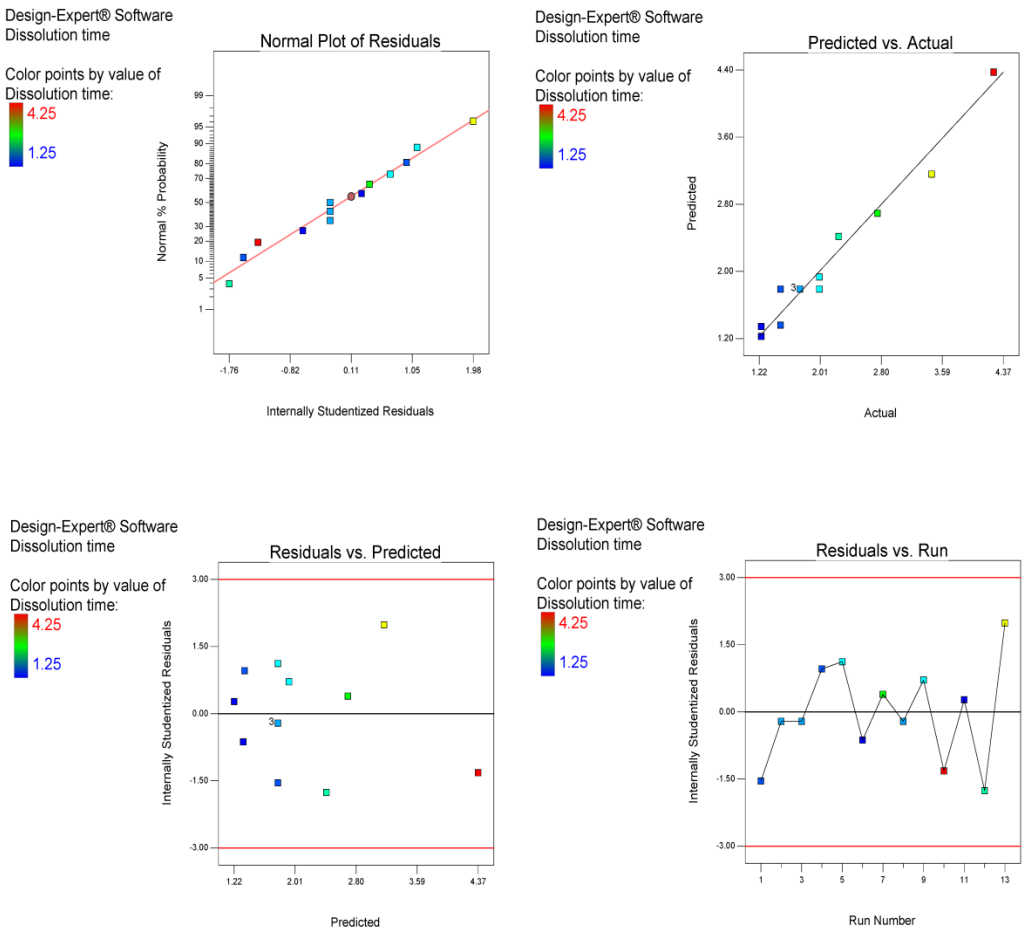

Figure 7.5: Residual plots for in-vitro dissolution time of cubosomes of TAC loaded MN Patch

Contour and response surface plots are presented in Fig. 7.6. This graph was used to depict how the in-vitro dissolution time is related to respective CMA.

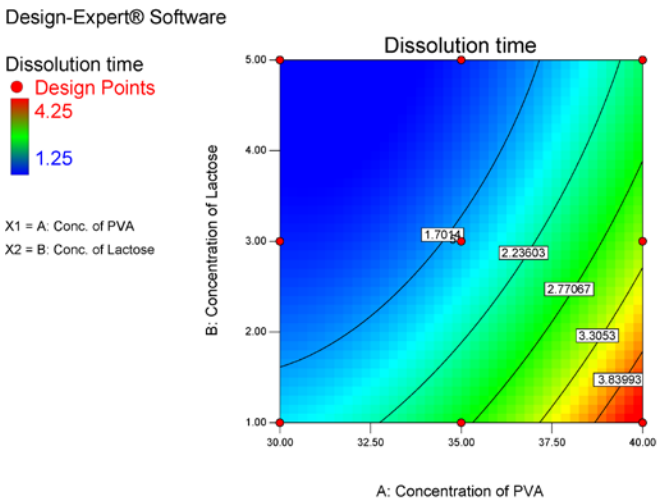

(A)

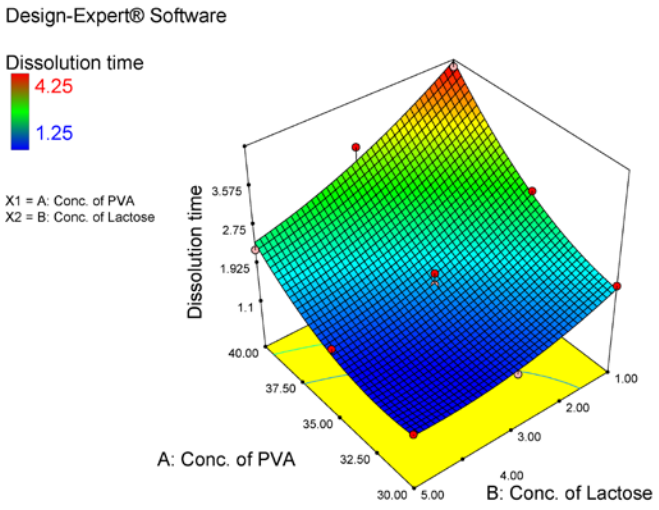

(B)

Figure 7.6: (A) Contour and (B) response surface plots for in-vitro dissolution time of cubosomes of TAC loaded MN Patch

Numerical and graphical optimizations were performed by the software for defined optimization criteria as presented in Table 7.13 and 7.14. Software was automated in a manner that it provides optimization solution wherein all the CMAs will be kept within experimental range.

Table 7.13: Criteria for numerical and graphical optimizations of cubosomes of TAC loaded MN Patch

CMA	Goal	Lower limit	Upper limit
Conc. of PVA	In range	30	40
Conc. of Lactose	In range	1	5
AFF	In range	0.5	1.5
In-vitro dissolution time	In range	0.0	2.0

Further, the desirability and overly plot is depicted in fig 7.7 and 7.8.

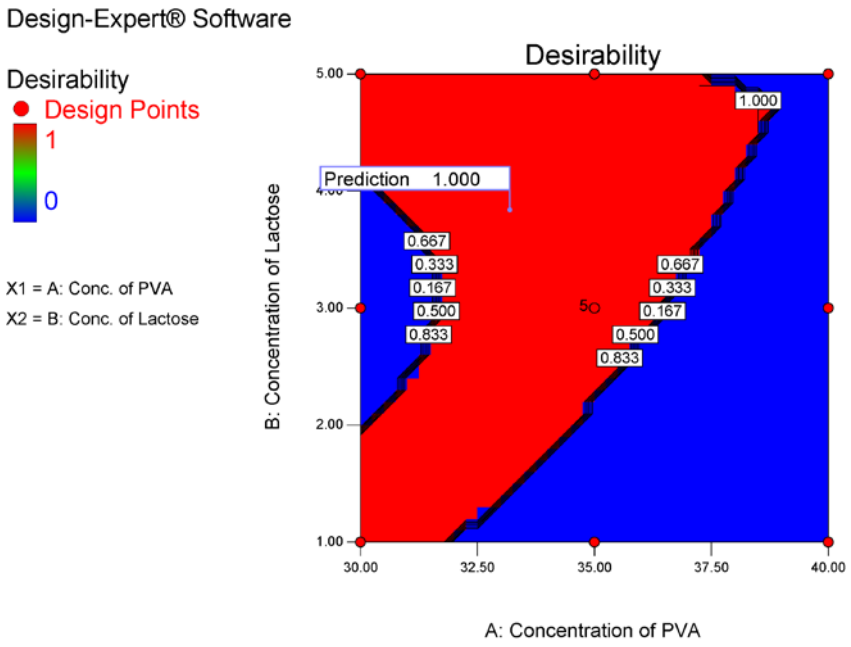

Figure 7.7: Desirability plot for the optimization of cubosomes of TAC loaded MN Patch

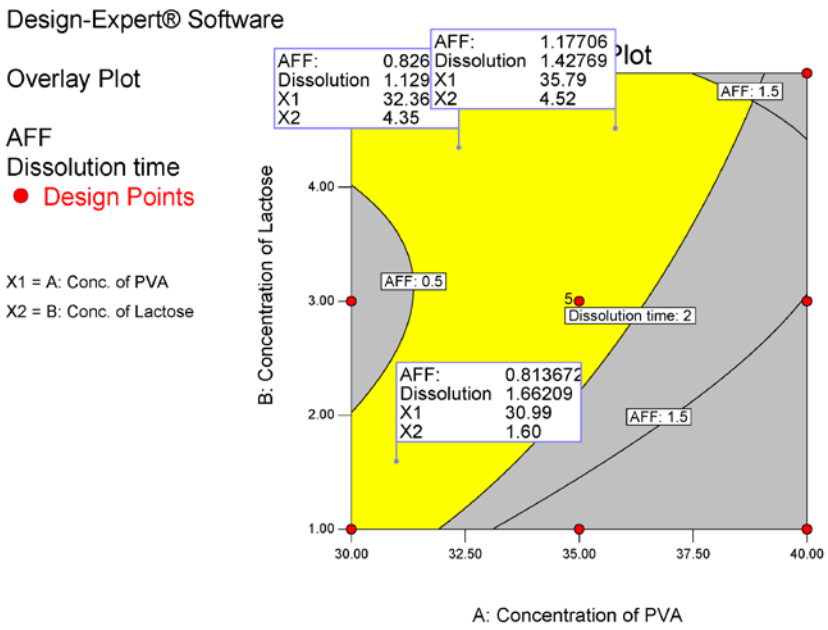

Figure 7.8: Overly plot for the optimization of cubosomes of TAC loaded MN Patch

7.3.6. Results of Checkpoint batch of cubosomes of Tacrolimus loaded Microneedle Patch

Upper limit and lower limit of the independent variables and CQAs at 95 % confidence and prediction level are given in table 7.14 & 7.15. Three checkpoint batches were prepared according to these levels and results of these checkpoint batches are represented in table 7.16. The legitimacy of the model was established as the average value of both CQA was observed to lie within low and high levels of 95% confidence interval.

Table 7.14: Levels of independent variables as per the point prediction analysis.

Factor	Name	Level	Low level	High level
A	Conc. of PVA	35.00	30.00	40.00
B	Conc. of Lactose	3.00	1.00	5.00

Table 7.15: Levels of responses at 95 % confidence and prediction intervals

Response	SE Mean	95 % CI* low	95 % CI* high	SE Pred	95 % PI* low	95 % PI* high
AFF (N)	0.091	0.64	1.07	0.24	0.29	1.42
Dissolution time (min)	0.086	1.59	1.99	0.22	1.26	2.32

*CI = Confidence interval; PI = prediction interval

Table 7.16: Results of checkpoint batches obtained using optimized overly plot of MN patch loaded with cubosomes of TAC

Sr. No.	Conc. PVA (% w/v)	Conc. of Lactose (%w/v)	Predicted value		Results obtained	
			AFF (N)	Dissolution time (min)	AFF (N)	Dissolution time (min)
1	32.36	4.35	0.83	1.13	1.06	1.25
2	35.79	4.52	1.17	1.42	1.24	1.50
3	30.99	1.60	0.81	1.66	0.95	1.50
Avg					1.08	1.42

7.3.7. Formulation optimization of cubosomes of Febuxostat loaded MN Patch by 3^2 Factorial Design

Based on qualitative risk assessment, two CMAs were identified and their relationship with CQAs were exhaustively investigated using 3^2 Factorial Design. 3^2 Factorial Design was found suitable as it facilitated the analysis of PVA and lactose along with numerous numerical variables. The low (-1), medium (0) and high (+1) levels of all three CMA are listed in Table 7.17.

Table 7.17: Various critical material attributes along with their levels for optimization of cubosomes of FBX loaded MN Patch by 3^2 Factorial Design

Independent variables (CMA)		Unit	Levels		
			-1	0	+1
A	Concentration	% w/v	30	35	40

	of PVA				
B	Concentration of Lactose	% w/v	5	7.5	10

A randomized matrix of thirteen batches was generated by Design-Expert 7.0 and presented in Table 7.18. These batches were formulated according to the respective run order and studied for CQA using the methods described earlier. Table 7.18 also represents the resulting CQA of these batches.

Table 7.18: Randomized design matrix for cubosomes of FBX loaded MN Patch using 3^2 factorial design with its CQA

Batch no.	Run order	Independent variables		AFF (N)	In-vitro dissolution time (min)
		A: Conc. of PVA % W/V	B: Conc. of Lactose %W/V		
F1	11	35	7.5	0.8	1.75
F2	4	35	7.5	0.75	2.0
F3	8	40	5.0	1.84	4.75
F4	1	35	10.0	1.26	1.25
F5	13	35	5.0	0.51	3.25
F6	6	30	7.5	0.66	1.25
F7	12	35	7.5	1.07	1.5
F8	9	35	7.5	0.67	1.5
F9	5	30	10.0	0.82	1.0
F10	2	40	10.0	4.06	2.5
F11	10	40	7.5	2.37	3.5
F12	7	35	7.5	0.81	1.5
F13	3	30	5.0	0.49	2.25

The experimental data of axial fracture force (AFF) and in-vitro dissolution time software suggests quadratic model for process order. Analysis of

variance (ANOVA) was performed by the same software. The categorization of terms as significant or insignificant was done on the basis of the p-value i.e. model term having p-value less than 0.05 (α-level) is significant while others are insignificant.(11) Hierarchy based deletion of insignificant model terms was done to streamline the model and obtain reduced equation. ANOVA and coded coefficients of Full model for AFF are mentioned in Table 7.19 and 7.20 respectively.

Table 7.19: ANOVA of full quadratic model for AFF

Source	Sum of Square	Degree of freedom	Mean square	F Value	p-Value > F	
Model	11.84	5	2.37	50.15	< 0.0001	Significant
Conc. of PVA	6.61	1	6.61	140.11	< 0.0001	Significant
Conc. of Lactose	1.81	1	1.81	38.44	0.0004	Significant
AB	0.89	1	0.89	18.91	0.0034	Significant
A^2	1.78	1	1.78	37.67	0.0005	Significant
B^2	0.082	1	0.082	1.74	0.2288	Not Significant
Residual	0.33	7	0.047			
Lack of fit	0.24	3	0.080	3.54	0.1268	Not significant
Pure error	0.090	4	0.023			
Cor total	12.17	12				

As showed in ANOVA table, concentration of PVA, Lactose and interaction between them were found to affect AFF significantly. An insignificant

lack-of fit showed the competence of the model in justifying the difference in the observations.

Table 7.20: Coded coefficients of full quadratic model for axial fracture force

Term	Full model		
	Coefficient	**SE Coefficient**	**VIF**
Intercept	0.79	0.090	-
A: Conc. of PVA	1.05	0.089	1.0
B: Conc. of Lactose	0.55	0.089	1.0
AB	0.47	0.11	1.0
A^2	0.80	0.13	1.17
B^2	0.17	0.13	1.17

Coefficients table for AFF showed VIF values near to 1 indicating that the predictors are not correlated and regression coefficients are well estimated.(12) Regression equation for full model in coded and uncoded units is presented as Eq. 7.7 & 7.8. The (+) and (-) symbol preceding every coefficient indicates a direct/ inverse relationship of the respective model term with AFF.

$$AFF = +0.79 + 1.05\ A + 0.55\ B + 0.47\ AB + 0.80\ A^2 + 0.17\ B^2$$

Equation- 7.7

Reduced model equation:

$$AFF = +0.79 + 1.05\ A + 0.55\ B + 0.47\ AB + 0.80A^2$$

Equation- 7.8

Regression equation for reduced model is presented in equation 7.9.

$$AFF = +0.790 + 1.05\ (\text{Conc. of PVA}) + 0.55\ (\text{Conc. of Lactose}) + 0.47\ (\text{Conc. of PVA})(\text{Conc. of Lactose}) + 0.80\ (\text{Conc. of PVA})^2$$

Equation- 7.9

Here, we observed that concentration of PVA and lactose have a positive effect on the AFF of MN patch loaded with cubosomes of FBX which means that as the concentration of PVA and lactose increases it also increases the AFF of MN patch loaded with cubosomes of FBX. Moreover, from reduced model 7.8 an interaction term B^2 was removed as its p value is greater than 0.05 as showed in table 7.19.

Model summary for AFF is mentioned in Table 7.21. A low SD value and high R^2 value symbolized an improved prediction of observations by the model. Assumed R^2 value was reported to be in close proximity with adjusted R^2 value for further supporting the prediction potential of the model.

Table 7.21: Summary of full quadratic model for AFF

Response	Full model			
	SD	R-sq	R-sq (adj)	R-sq (pred)
AFF (N)	0.22	0.9728	0.9534	0.7977

Four different residual plots viz., normal plot of residual, residual versus ascending predicted response values, residual versus experimental run order and predicted versus actual were generated for AFF and presented in fig. 7.9. It was observed that the data was normally distributed in normal plot as it could be seen that the residuals followed a straight line. Further, the prediction of constant variance was validated as random scattering with the absence of any megaphone pattern in residual versus predicted plot was seen. Likewise, the absence of lurking variables was validation by the random scattering lacking any pattern in residual versus run plot. The selected model gave convenient assumption of the values given that the data points were consistently split by 45-degree line.(13)

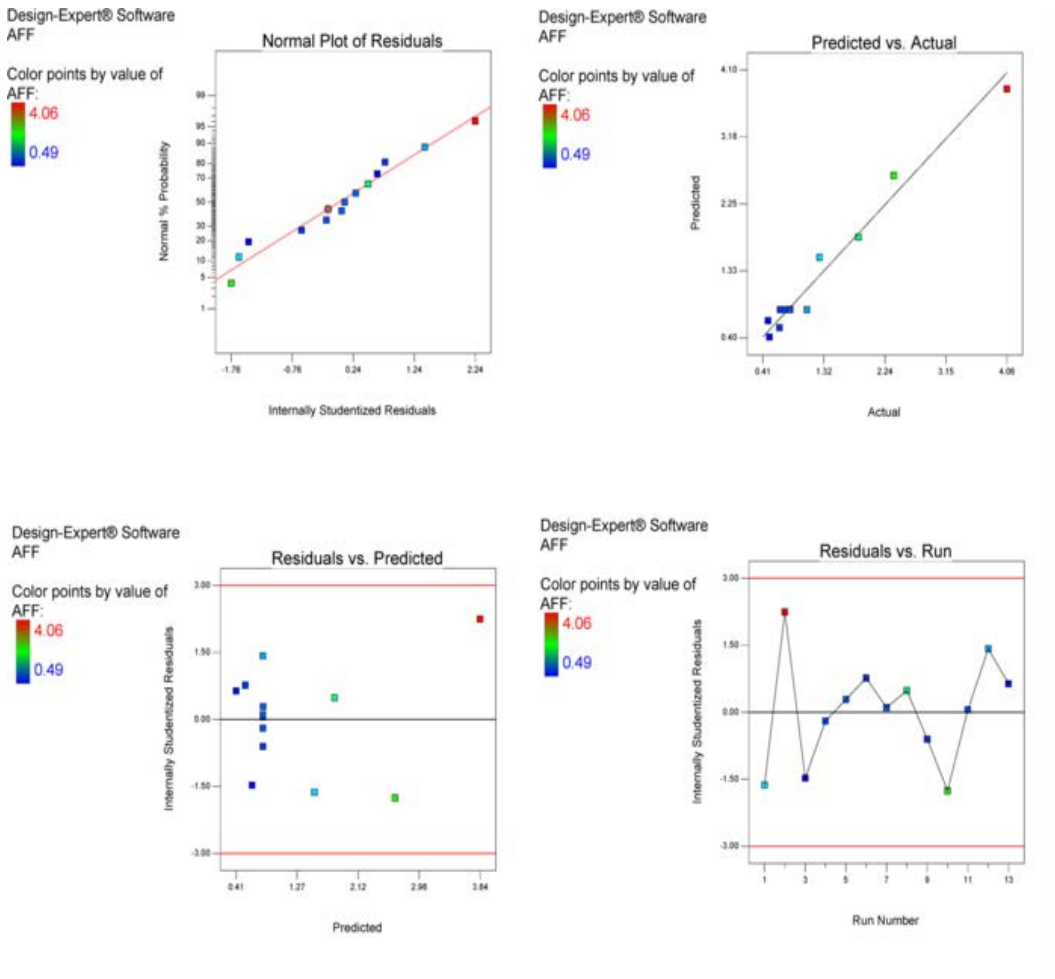

Figure 7.9: Residual plots for AFF of cubosomes of FBX loaded MN Patch

Contour and response surface plots are presented in Fig. 7.10. This graph was used to depict how the AFF is related to respective CMA.

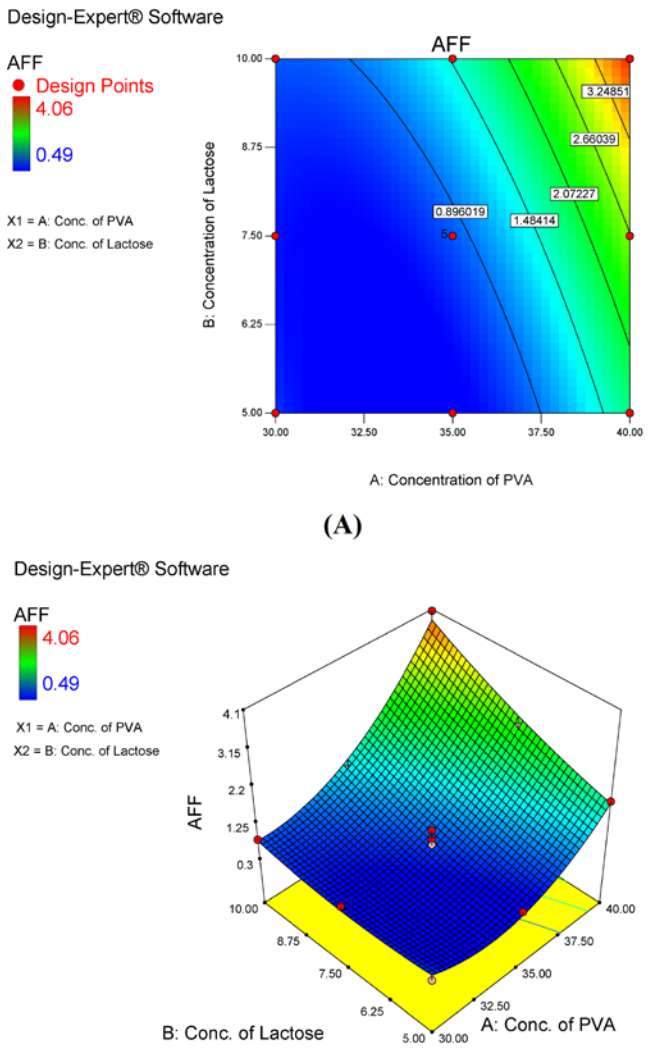

Figure 7.10: (A) Contour and (B) response surface plots for AFF of cubosomes of FBX loaded MN Patch

ANOVA and coded coefficients of Full model for in-vitro dissolution time are mentioned in Table 7.22 and Table 7.23, respectively.

Table 7.22: ANOVA of full quadratic model for in-vitro dissolution time

Source	Sum of Square	Degree of freedom	Mean square	F Value	p-Value > F	
Model	13.99	5	2.80	60.06	< 0.0001	Significant
Conc. of PVA	6.51	1	6.51	139.73	< 0.0001	Significant
Conc. of Lactose	5.04	1	5.04	108.21	< 0.0001	Significant
AB	0.25	1	0.25	5.37	0.0537	Not Significant
A^2	0.85	1	0.85	18.33	0.0037	Significant
B^2	0.51	1	0.51	11.01	0.0128	Significant
Residual	0.33	7	0.047			
Lack of fit	0.13	3	0.042	0.84	0.5382	Not significant
Pure error	0.20	4	0.050			
Cor total	14.32	12				

As showed in ANOVA table, concentration of PVA, Lactose and interaction between them were found to affect in-vitro dissolution time significantly. An insignificant lack-of fit showed the competence of the model in justifying the difference in the observations. The categorization of terms as significant or insignificant was done on the basis of the p-value i.e. model term having p-value less than 0.05 (α-level) is significant while others are insignificant.(11)

Table 7.23: Coded coefficients of full quadratic model for in-vitro dissolution time

Term	Full model		
	Coefficient	**SE Coefficient**	**VIF**
Intercept	1.70	0.090	-
A: Conc. of PVA	1.04	0.088	1.0
B: Conc. of Lactose	-0.92	0.088	1.0
AB	-0.25	0.11	1.0
A^2	0.56	0.13	1.17
B^2	0.43	0.13	1.17

Coefficients table for in-vitro dissolution time showed VIF values near to 1 indicating that the predictors are not correlated and regression coefficients are well estimated.(12) Regression equation for full model in coded and uncoded units is presented as Eq. 7.10 & 7.11. The (+) and (-) symbol preceding every coefficient indicates a direct or inverse relationship of the respective model term with AFF.

$$\text{In-vitro dissolution time} = +1.70 + 1.04\,A - 0.92\,B - 0.25\,AB + 0.56\,A^2 + 0.43\,B^2$$

Equation- 7.10

Reduced model Equation:

$$\text{In-vitro dissolution time} = +1.70 + 1.04A - 0.92B + 0.56A^2 + 0.43B^2$$

Equation- 7.11

Regression equation for reduced model is presented in equation 7.12.

$$\text{In-vitro dissolution time} = +1.70 + 1.04\,(\text{Conc. of PVA}) - 0.92\,(\text{Conc. of Lactose}) + 0.56\,(\text{Conc. of PVA})^2 + 0.43\,(\text{Conc. of Lactose})^2$$

Equation- 7.12

From the equation 7.10, it can be concluded that concentration of PVA has a positive effect on the in-vitro dissolution time of MN patch means as the concentration of PVA increases in-vitro dissolution time of a MN patch also increases. Opposite phenomena was observed with the concentration of lactose. Moreover interaction effect of concentration of lactose was not observed on in-vitro dissolution time of MN patch. Thus, in reduced model equation 7.11, interaction AB was removed because it has a p value greater than 0.05 as shown in table 7.22.

Model summary for in-vitro dissolution time is presented in Table 7.24. A low SD value and high R^2 value symbolized an improved prediction of observations by the model. Assumed R^2 value was reported to be in close proximity with adjusted R^2 value for further supporting the prediction potential of the model.

Table 7.24: Summary of full quadratic model for in-vitro dissolution time

Response	**Full model**			
	SD	**R-sq**	**R-sq (adj)**	**R-sq (pred)**
In-vitro dissolution time (min)	0.22	0.9772	0.9609	0.9098

Four different residual plots viz., normal plot of residual, residual versus ascending predicted response values, residual versus experimental run order and predicted versus actual were generated for in-vitro dissolution time and presented in Fig. 7.11. It was observed that the data was normally distributed in normal plot as it could be seen that the residuals followed a straight line. Further, the prediction of constant variance was validated as random scattering with the absence of any megaphone pattern in residual versus predicted plot was seen. Likewise, the absence of lurking variables was validation by the random scattering lacking any pattern in residual versus run plot. The selected model gave convenient assumption of the values given that the data points were consistently split by 45-degree line.(13)

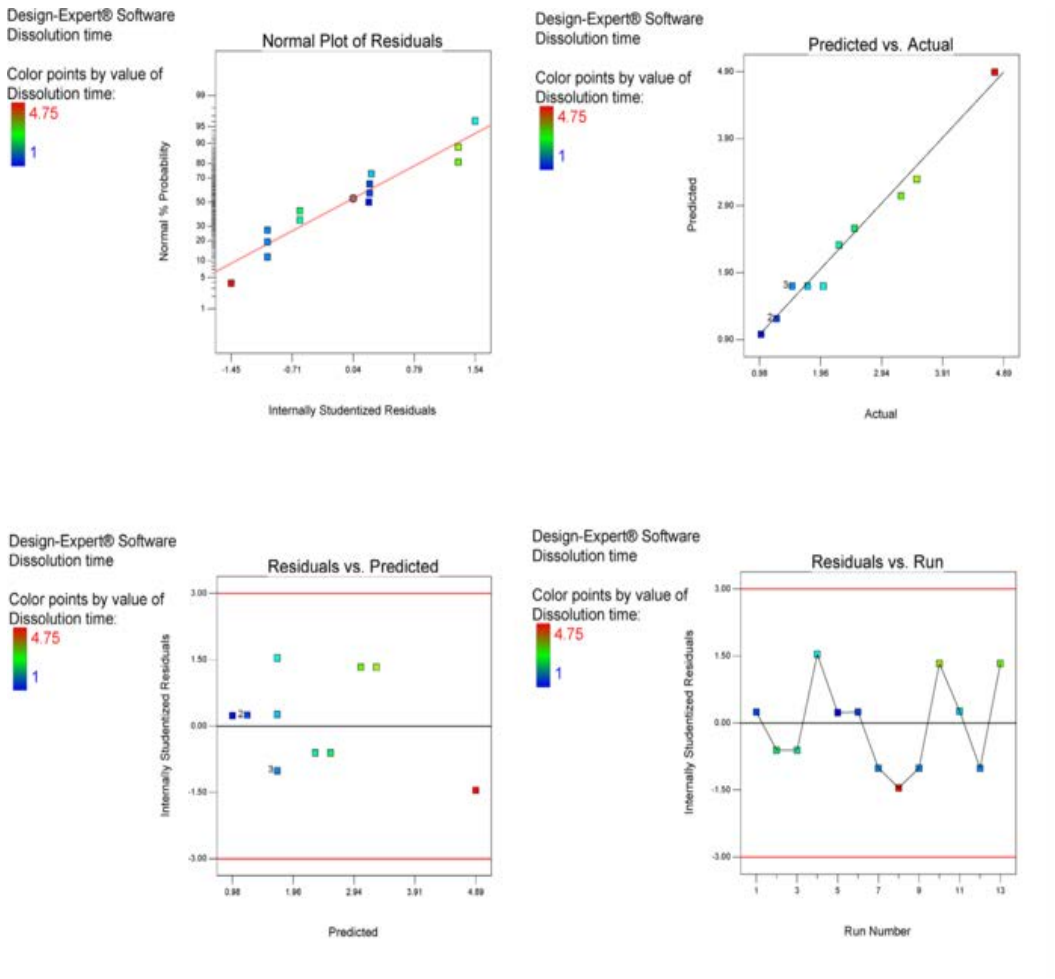

Figure 7.11: Residual plots for in-vitro dissolution time of cubosomes of FBX loaded MN Patch

Contour and response surface plots are presented in Fig. 7.12. This graph was used to depict how the in-vitro dissolution time is related to respective CMA.

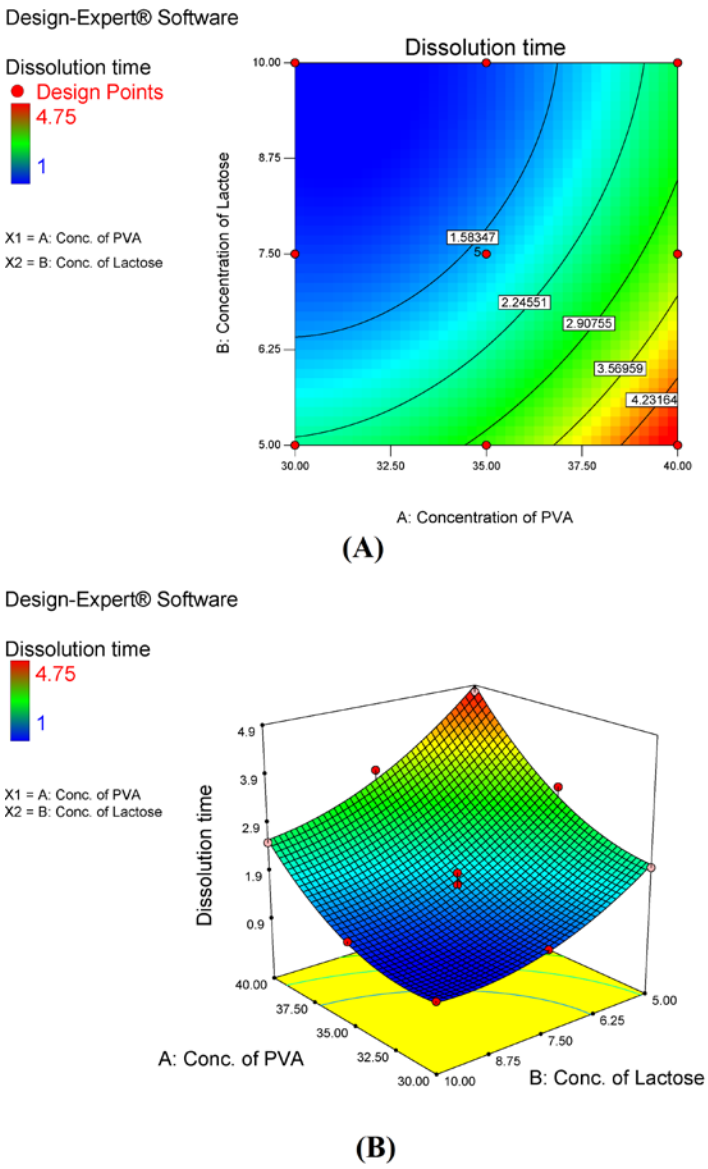

Figure 7.12: (A) Contour and (B) response surface plots for in-vitro dissolution time of cubosomes of FBX loaded MN Patch

Numerical and graphical optimizations were performed by the software for defined optimization criteria as presented in Table 7.25. The software was formulated in a manner to provide optimization solution wherein all the CMAs are kept in experimental range.

Table 7.25: Criteria for numerical and graphical optimizations of cubosomes of FBX loaded MN Patch

CMA	Goal	Lower limit	Upper limit
Conc. of PVA	In range	30	40
Conc. of Lactose	In range	1	5
AFF	In range	0.5	1.5
In-vitro dissolution time	In range	0.0	2.0

Further, desirability and overly plot is depicted in fig 7.13 and 7.14.

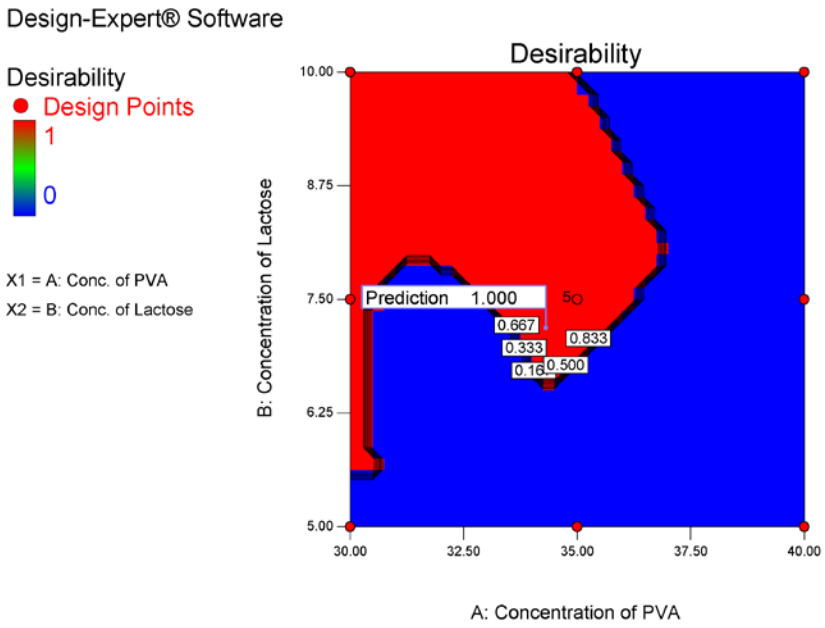

Figure 7.13: Desirability plot for the optimization of cubosomes of FBX loaded MN Patch

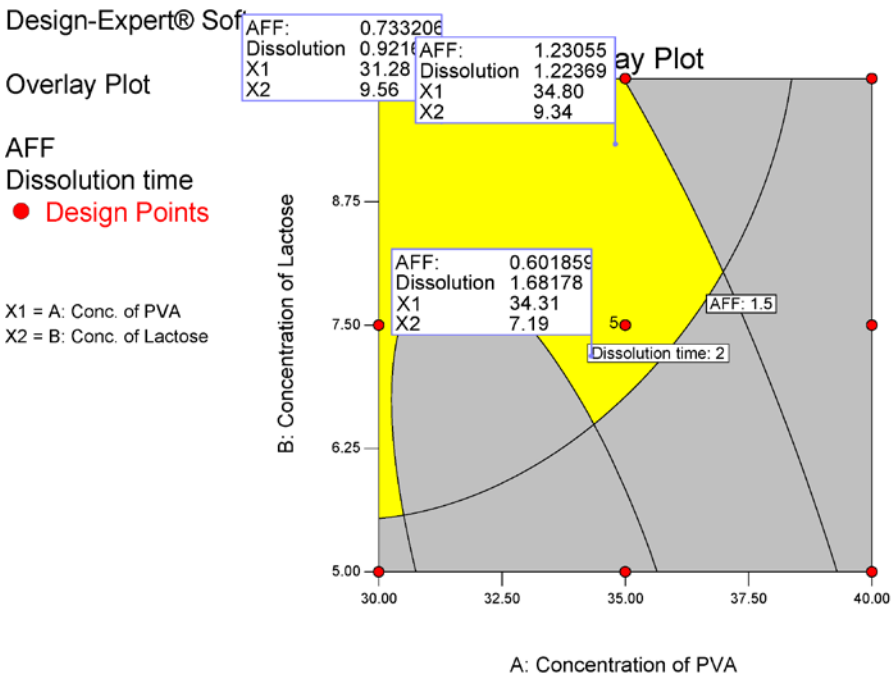

Figure 7.14: Overly plot for the optimization of cubosomes of FBX loaded MN Patch

The desirability plot showed a desirability of 1.000 for the solution provided by the software.

7.3.8. Results of Checkpoint batch of cubosomes of Febuxostat loaded Microneedle Patch

Upper limit and lower limit of the independent variables and CQAs at 95 % confidence and prediction level are given in table 7.26 & 7.27. Three checkpoint batches are prepared according to these levels and results of these checkpoint batches are represented in table 7.28. The legitimacy of the model was established as it was found that the average value of both CQA falls within low and high levels of 95% confidence interval.

Table 7.26: Levels of independent variables as per the point prediction analysis

Factor	Name	Level	Low level	High level
A	Conc. of PVA	34.31	30.00	40.00

B	Conc. of Lactose	7.19	5.0	10.00

Table 7.27: Levels of responses at 95 % confidence and prediction intervals

Response	SE Mean	95 % CI* low	95 % CI* high	SE Pred	95 % PI* low	95 % PI* high
AFF (N)	0.09	0.39	0.81	0.24	0.46	1.16
Dissolution time (min)	0.089	1.47	1.89	0.23	1.13	2.23

*CI = Confidence interval; PI = prediction interval

Table 7.28: Results of checkpoint batches obtained using optimized overly plot of FBX loaded cubosomes

Sr. No.	Conc. PVA (% w/v)	Conc. of Lactose (%w/v)	Predicted value		Results obtained	
			AFF (N)	Dissolution time (min)	AFF (N)	Dissolution time (min)
1	31.28	9.56	0.73	0.92	0.82	1.00
2	34.80	9.34	1.23	1.22	1.19	1.00
3	34.31	7.19	0.60	1.68	0.59	1.75
Avg					0.86	1.25

7.3.9. In-vitro characterization of cubosomes loaded fast dissolving Microneedle Patch

7.3.9.1.Axial Fracture Force

Axial fracture force of MN Patch containing cubosomes of TAC and FBX was calculated using the following equation; which was found to be 1.16 N and 1.2 N respectively. A prepared MN patch should have sufficient mechanical strength i.e. 0.03 N/microneedle so that it can breach the stratum corneum layer of a skin and deliver the loaded carrier systems directly to the dermis layer of a skin.(14) From this dermis layer of a skin, the drug can be absorbed directly in a systemic circulation. Thus, it can be interpreted that the prepared MN patch of cubosomes of FBX has a required minimum mechanical strength according to the literature.(14)

$$F=mg$$

Where: m = mass applied for breaking of MN

g = gravitational force

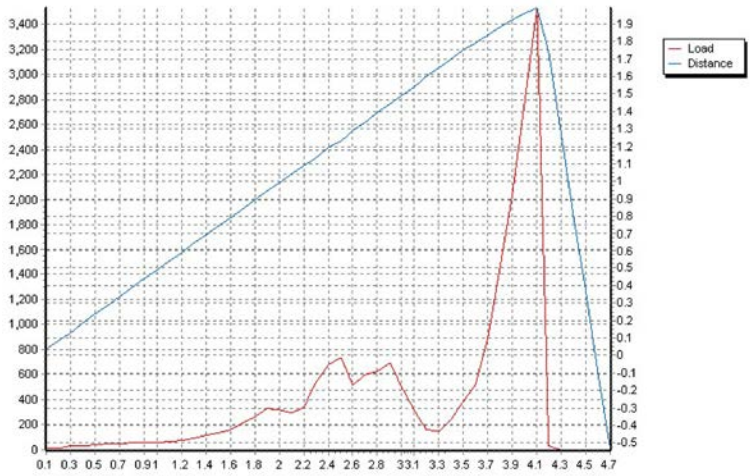

Figure 7.15: Load vs Time curve for MN patch loaded with cubosomes of TAC

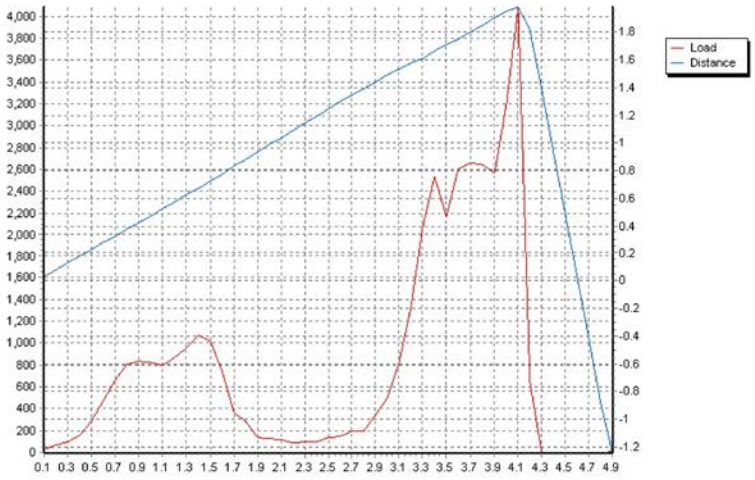

Figure 7.16: Load vs Time curve for MN patch loaded with cubosomes of FBX

7.3.9.2.In-vitro dissolution study

In-vitro dissolution time of prepared MN Patches containing cubosomes of TAC and FBX was performed and found out to be 1.50 and 1.25 min respectively

as shown in fig 7.17 and 7.18. After dissolution of a MN in the skin a drug in it will release to the dermis layer. Sooner the MN dissolve in the skin faster it is available for the systemic circulation. Here, the prepared MN patches release drug to the dermis layer in less than 2 min and it is available for the systemic absorption.

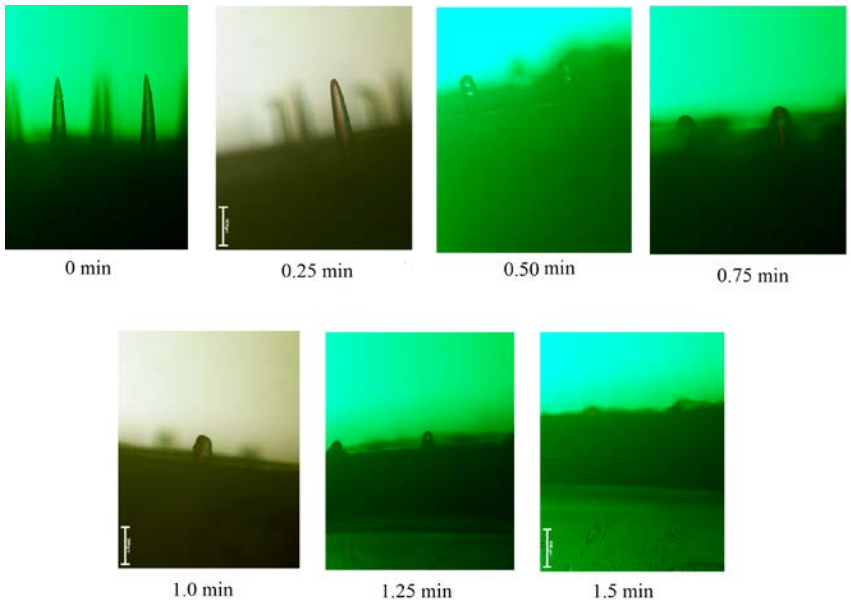

Figure 7.17: In-vitro dissolution study of MN patch containing TAC loaded cubosomes

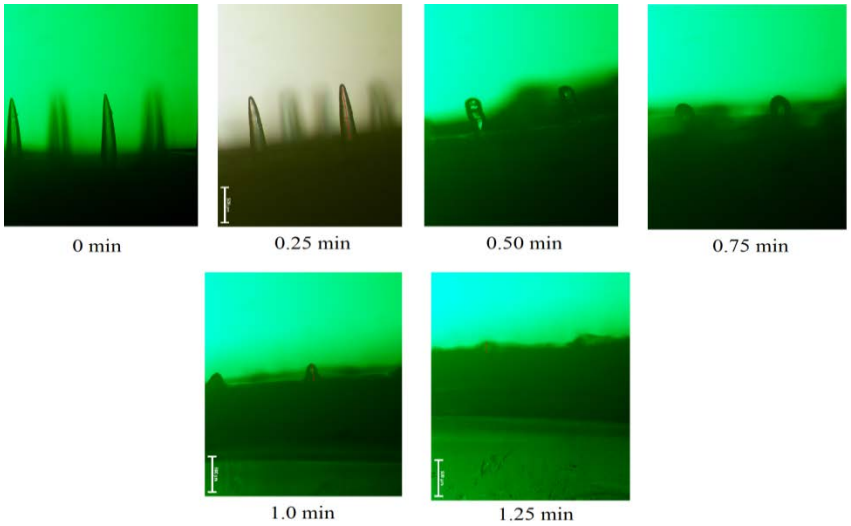

Figure 7.18: In-vitro dissolution study of MN patch containing FBX loaded cubosomes

7.3.9.3.Shape and surface morphology

SEM images of fast dissolving MN Patch are presented in Fig. 7.19 and 7.20. These images showed smooth surfaced, conical microneedles having a length of 1.5 mm, and a base diameter of approx. 200 µm. The microneedle array geometry observed in SEM images was suitable for skin piercing with minimal damage as available in literature.(3, 6) Smooth texture of both prepared MN patches suggests that in both MN patches prepared cubosomal dispersion TAC/FBX was successfully incorporated. Moreover, top view of MN patch, a distance between two microneedles can be easily observed.

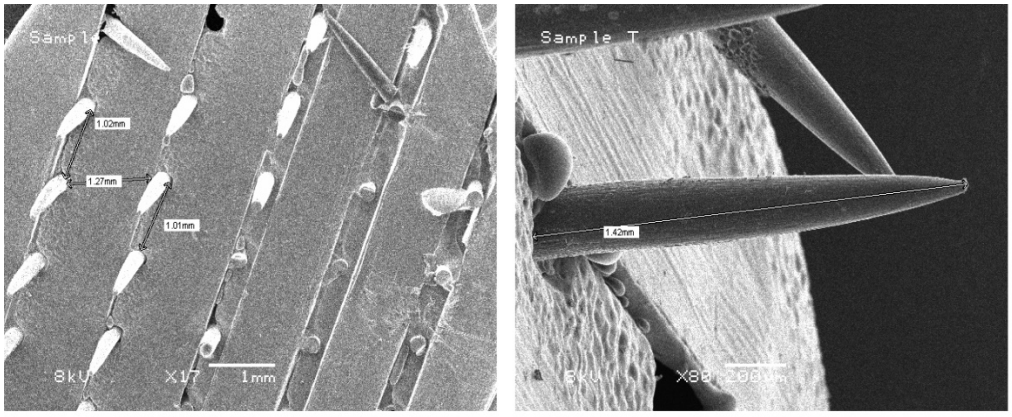

(A) (B)

Figure 7.19: SEM of MN patch loaded with cubosomes of TAC (A) Top view (B) Side view

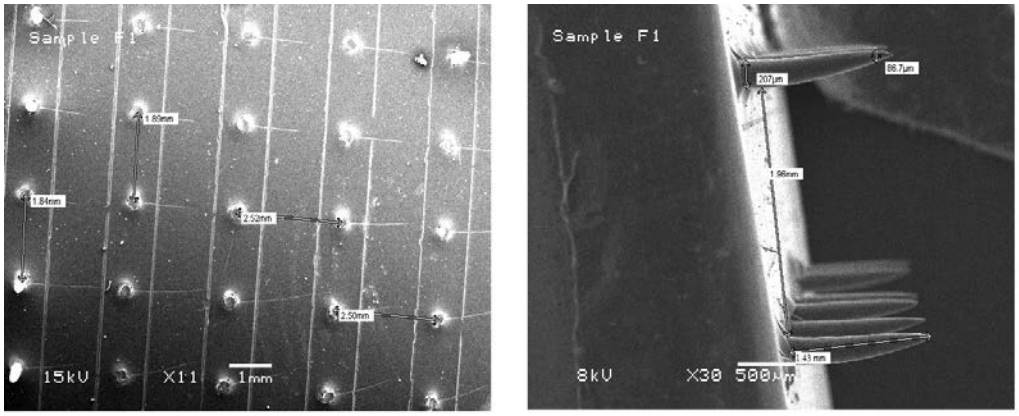

(A) (B)

Figure 7.20: SEM of MN patch loaded with cubosomes of FBX (A) Top view (B) Side view

7.3.9.4.Skin penetrability

Skin penetrability of prepared MN Patches containing cubosomes of TAC and FBX are shown in fig 7.22 A & B respectively. The presence of small dark blue spots on the rat skin as shown in fig 7.22 A and B are indicative of the fact that prepared microneedles were successful in penetrating rat skin and overcame the barrier of stratum corneum. It can be concluded that microneedles successfully delivered the drug directly to the dermis layer of skin.

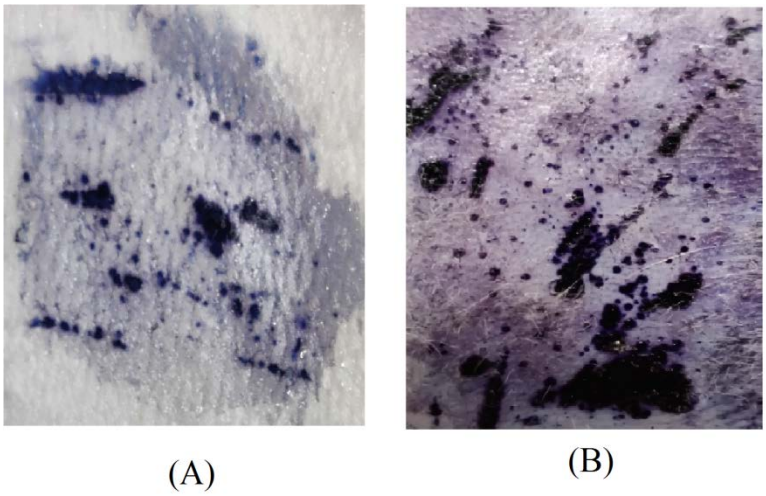

Figure 7.21: Skin penetrability of (A) Cubosomes of TAC loaded MN Patch and (B) Cubosomes of FBX loaded MN Patch

7.3.9.5.Pore closure kinetic

Application of MN patch on rat skin formed pores which were detected using microscope and its average pore diameter were measured and summarized in Table 7.29 and 7.30. Moreover, Fig. 7.22 & 7.23 represents images of pores formed in skin due to the application MN patch containing cubosomes of TAC and MN patch loaded with FBX cubosomes respectively at 4X and 10X microscopic zoom. Form the data obtained and fig 7.22 & 7.23, it can be concluded that the pores formed using fast dissolving MN patch remained open for 24 hours under occlusive conditions.

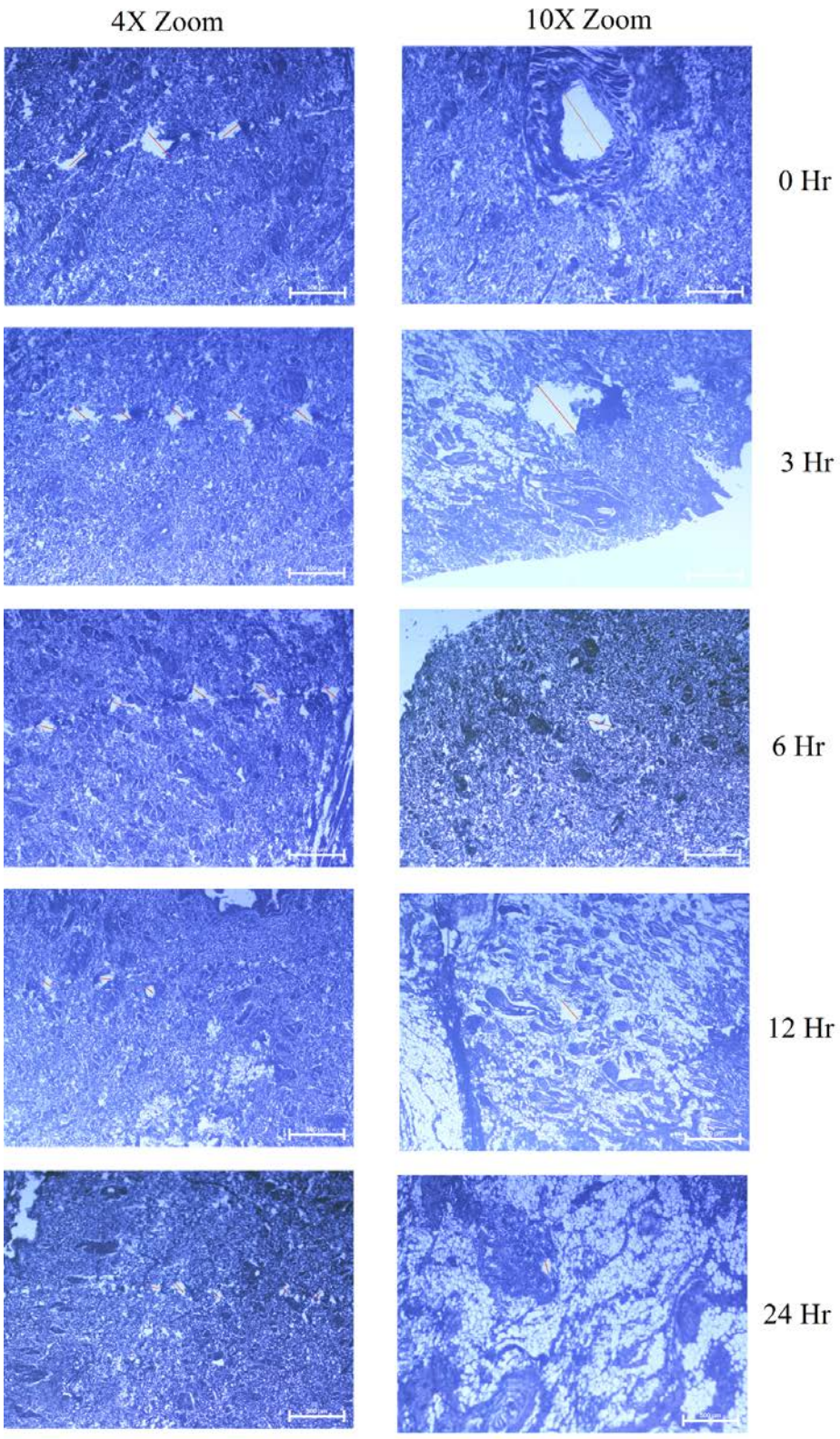

Figure 7.22: Pore closure kinetics for MN patch loaded with cubosomes of TAC

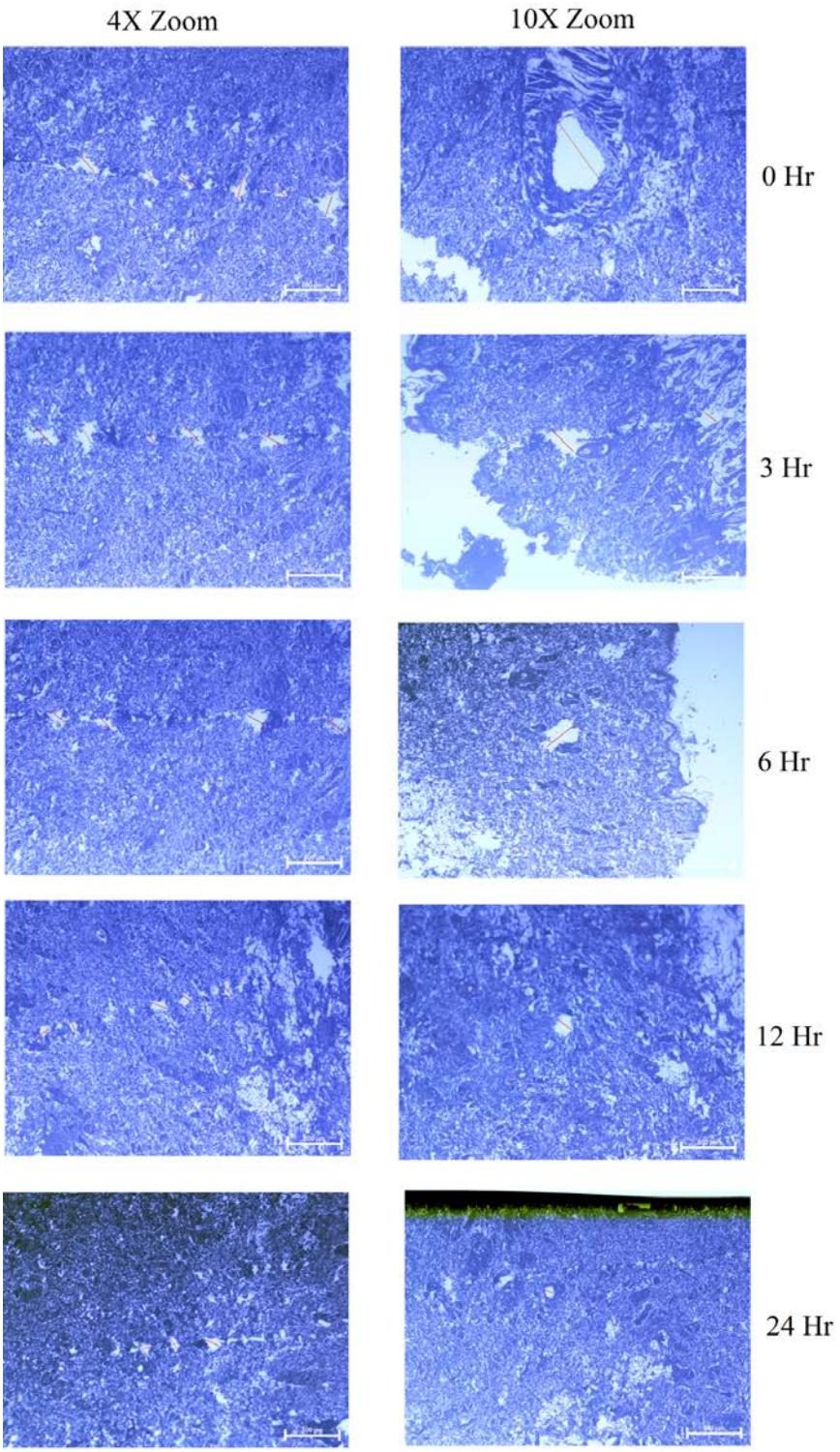

Figure 7.23: Pore closure kinetics for MN patch loaded with cubosomes of FBX

Table 7.29: Pore closure kinetic at different time intervals for MN patch loaded with cubosomes of TAC

Sr no	Time (h)	Average pore diameter (µm)
1	0	153.33 ± 4.59
2	3	132.37 ± 3.32
3	6	114.77 ± 2.52
4	12	88.77 ± 2.20
5	24	46.94 ± 1.87

*Values represented as mean ± SD

Table 7.30: Pore closure kinetic at different time intervals for MN patch loaded with cubosomes of FBX

Sr no	Time (h)	Average pore diameter (µm)
1	0	163.59 ± 5.75
2	3	139.20 ± 3.21
3	6	120.41 ± 2.77
4	12	93.23 ± 2.07
5	24	52.30 ± 1.31

*Values represented as mean ± SD

7.3.9.6.Physical stability of cubosomes in fast dissolving microneedle patch

The TEM images of cubosomal dispersions obtained after their MN Patch dissolution are presented in Fig. 7.24. These images showed retention of morphological characteristics of cubosomes indicating their stability within the MN Patch. Similarly, no significant difference was observed in mean vesicle size as well as entrapment efficiency of cubosomes compare to the previous results shown table 7.31, which also suggests stability of prepared cubosomal dispersion MN patches.

Table 7.31: Size and entrapment data of cubosomes after dissolution of MN Patch compare to previous results shown in chapter 5 & 6.

Formulation	Vesicle size (nm)		% Entrapment efficiency	
	Initial	After disso. of MN Patch	Initial	After disso. of MN Patch
Cubosomes of FBX	157.5 ± 4.16	154 ± 3.94	85.2 ± 2.68	84.9 ± 1.88
Cubosomes of TAC	223.8 ± 6.84	222.6 ± 7.41	92.78 ± 3.55	91.57 ± 2.37

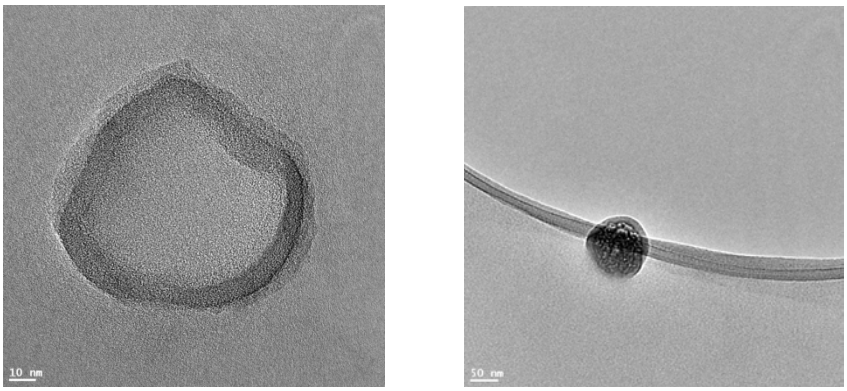

(A) **(B)**

Figure 7.24: TEM of cubosomes after dissolving MN patch in water (A) For FBX (B) TAC

7.3.9.7.Total drug content

Total drug content of MN Patch containing TAC and FBX cubosomes was found to be 96.23 % and 98.14 % respectively.

7.3.9.8.*In vitro drug release*

In vitro drug release from plain drug loaded MN patch and cubosomes loaded MN patches were investigated and the data obtained for cumulative percent drug release at various time points are presented in Table 7.31 as well as depicted in Fig. 7.25 & 7.26. Release data of all four formulations suggested that more than 50 % drug was released in first one hour only while more than 90 % drug was released in 2 hours. The results showed significant increase in drug release when it compared to drug release profile of respective cubosomal

dispersions (refer chapter 5 section 5.3.7.8 and 6 section 6.3.7.8). The optimized MN patches were able to penetrate the diffusion bag due its microneedle structure. Then, the microneedles were dissolved in diffusion medium and able to release drug in diffusion medium rapidly. Whereas in case of cubosomes, drug have to diffused through the diffusion bag which is time taking process and thus it releases drug slowly. Because of this reason such drastic increase in percent drug release obtained with MN patches of both drugs compared to its cubosomal dispersion.

Table 7.31: In vitro release profile of drug from its drug and cubosomes loaded MN patch

Time (h)	Cumulative percent drug released			
	MN patch of TAC	MN patch of TAC cubosomes	MN patch of FBX	MN patch of FBX cubosomes
0.5	54.34 ± 2.28	60.19 ± 2.39	60.06 ± 2.76	62.08 ± 2.27
1	63.33 ± 1.72	69.35 ± 2.12	67.99 ± 2.46	71.47 ± 2.32
1.5	76.52 ± 1.02	79.22 ± 2.65	75.78 ± 1.72	89.87 ± 2.69
2	90.18 ± 4.00	92.84 ± 3.52	87.44 ± 3.00	91.68 ± 4.05
3	94.07 ± 4.03	93.33 ± 2.94	91.19 ± 4.07	92.89 ± 3.70
4	95.52 ± 5.04	93.99 ± 3.13	91.50 ± 4.02	93.38 ± 3.39
5	96.04 ± 4.43	94.20 ± 2.94	92.04 ± 3.60	93.54 ± 3.51
6	96.32 ± 4.54	94.66 ± 3.80	92.58 ± 4.06	93.92 ± 3.39
7	96.84 ± 4.32	95.22 ± 3.31	93.16 ± 3.84	94.63 ± 3.35
8	95.82 ± 4.31	95.69 ± 3.41	93.48 ± 3.56	94.62 ± 2.72
9	95.97 ± 3.84	95.88 ± 3.74	93.89 ± 3.54	95.10 ± 3.01
10	96.26 ± 4.13	96.29 ± 3.81	94.37 ± 3.31	95.36 ± 2.80
11	96.78 ± 4.25	97.06 ±3.21	94.68 ± 3.84	95.39 ± 2.97
12	96.69 ± 4.64	97.40 ± 4.01	95.04 ± 3.17	95.49 ± 2.76
24	97.01 ± 4.42	97.64 ± 4.69	94.92 ± 2.16	95.43 ± 2.36

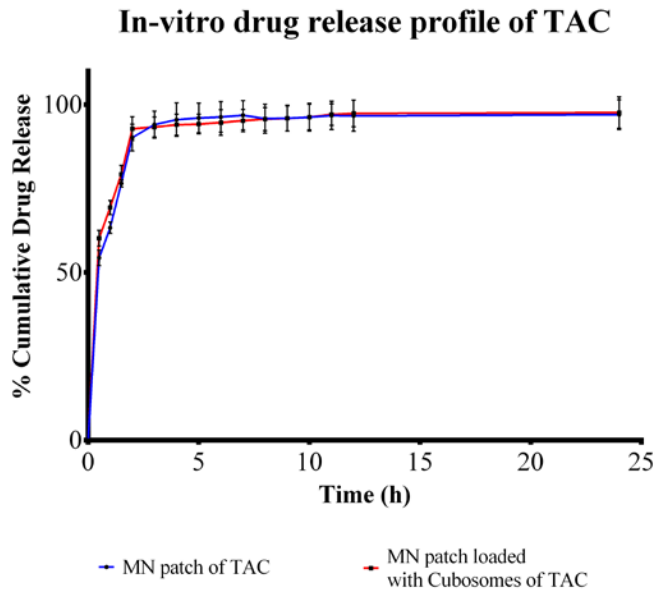

Figure 7.25: In-vitro drug release from developed MN patch formulation of TAC

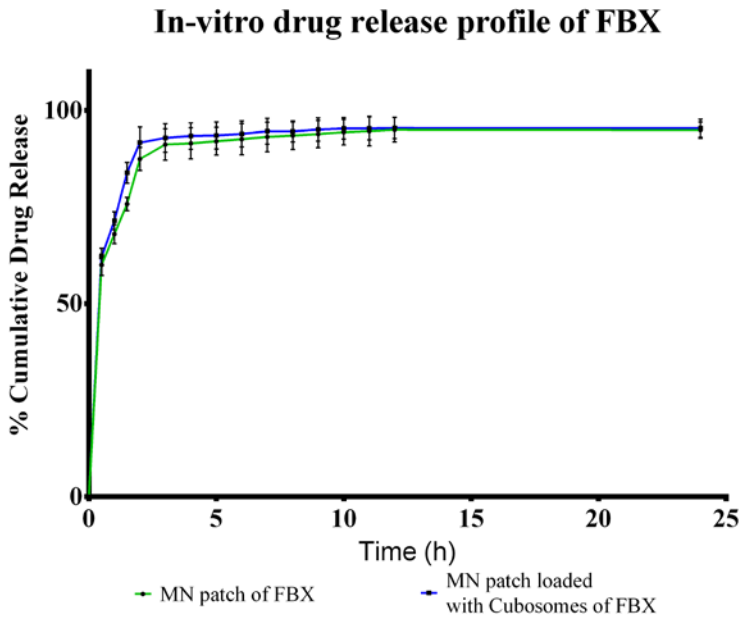

Figure 7.26: In-vitro drug release from developed MN patch formulation of FBX

The result of various mathematical models, applied to understand the drug release kinetics from drug and cubosomes loaded MNP, are summarized in Table 7.32. The R^2 value for first order model was found higher which suggest that release rate is dependent on remaining drug concentration within the carrier.

Table 7.32: Various mathematical models and their correlation coefficient values

Mathematical models		MN patch of TAC	MN patch of TAC cubosomes	MN patch of FBX	MN patch of FBX cubosomes
Zero order	**R^2**	0.5503	0.5815	0.6601	0.5432
First order		0.9818	0.9696	0.9719	0.9801
Higuchi		0.7175	0.7406	0.7631	0.7074
Hixon Crowell		0.8081	0.8187	0.8492	0.7902
Korsmeyer Peppas		0.8372	0.8570	0.8778	0.8339
	n	0.120	0.102	0.104	0.088

7.4 References

1. Park J-H, Allen MG, Prausnitz MR. Biodegradable polymer microneedles: fabrication, mechanics and transdermal drug delivery. Journal of controlled release. 2005;104(1):51-66.

2. Su L-C, Chen M-C. Efficient delivery of nanoparticles to deep skin layers using dissolvable microneedles with an extended-length design. Journal of Materials Chemistry B. 2017;5(18):3355-63.

3. Mönkäre J, Pontier M, van Kampen EE, Du G, Leone M, Romeijn S, et al. Development of PLGA nanoparticle loaded dissolving microneedles and comparison with hollow microneedles in intradermal vaccine delivery. European Journal of Pharmaceutics and Biopharmaceutics. 2018;129:111-21.

4. Lawrence XY. Pharmaceutical quality by design: product and process development, understanding, and control. Pharmaceutical research. 2008;25(4):781-91.

5. Thakkar H, Pandya K, Patel B. Microneedle-mediated transdermal delivery of tizanidine hydrochloride. Drug Delivery Systems: Springer; 2020. p. 239-58.

6. Li Z, He Y, Deng L, Zhang Z-R, Lin Y. A fast-dissolving microneedle array loaded with chitosan nanoparticles to evoke systemic immune responses in mice. Journal of Materials Chemistry B. 2020;8(2):216-25.

7. Lee JW, Park J-H, Prausnitz MR. Dissolving microneedles for transdermal drug delivery. Biomaterials. 2008;29(13):2113-24.

8. Srivastava PK, Thakkar HP. Vinpocetine loaded ultradeformable liposomes as fast dissolving microneedle patch: Tackling treatment challenges of dementia. European Journal of Pharmaceutics and Biopharmaceutics. 2020;156:176-90.

9. Eriksson L, Johansson E, Kettaneh-Wold N, Wikström C, Wold S. Design of experiments. Principles and Applications, Learn ways AB, Stockholm. 2000.

10. Indermun S, Choonara YE, Kumar P, du Toit LC, Modi G, van Vuuren S, et al. Ex vivo evaluation of a microneedle array device for transdermal application. International journal of pharmaceutics. 2015;496(2):351-9.

11. Sangshetti JN, Deshpande M, Zaheer Z, Shinde DB, Arote R. Quality by design approach: Regulatory need. Arabian Journal of Chemistry. 2017;10:S3412-S25.

12. 10.7 - Detecting Multicollinearity Using Variance Inflation Factors [cited 2021 7th June]. Available from: https://online.stat.psu.edu/stat462/node/180/.

13. Diagnostics Plots¶ [cited 2021 7th June]. Available from: https://www.statease.com/docs/v11/contents/analysis/diagnostics/diagnostics-plots/.

14. Olatunji O, Das DB, Garland MJ, Belaid L, Donnelly RF. Influence of array interspacing on the force required for successful microneedle skin penetration: theoretical and practical approaches. Journal of pharmaceutical sciences. 2013;102(4):1209-21.